Analysis of the Fluvial Stratigraphic Response to the Paleocene-Eocene Thermal Maximum in the Bighorn Basin, USA

Amanda Owen[1], Adrian J. Hartley[2], Trevor B. Hoey[3], Alena Ebinghaus[2], David W. Jolley[2], and Gary S. Weissmann[4]

[1]School of Geographical and Earth Sciences, University of Glasgow, G12 8QQ, UK

[2]Department of Geology and Petroleum Geology, University of Aberdeen, AB24 3UE, UK

[3]Department of Civil and Environmental Engineering, Brunel University London, Uxbridge, UB8 3PH, UK

[4]Department of Earth and Planetary Sciences, University of New Mexico, New Mexico, 87131-0001, USA

ABSTRACT

Geological deposits can reveal how environments of the past have responded to climate change, enabling important insights into how environments may respond to our current anthropogenically induced warming. The Paleocene-Eocene Thermal Maximum (PETM) occurred ca. 56 Ma and was a short-lived (approximately 200,000 years) global warming event (5-8°C rise). The PETM has been investigated at several terrestrial and marine localities across the globe. However, many studies are based on single successions, with very few sites being placed within a well-defined spatial and temporal context and with comparisons limited to deposits that lie immediately above and below the event. Due to the inherent variability of sedimentary systems, it is imperative that the appropriate context is provided to fully understand the impacts of climate change on landscapes and subsequent deposits. This study examines 28 locations, totaling over 4 km of recorded stratigraphy, within a newly defined quantified sedimentary basin context (Bighorn Basin, USA) to evaluate variability of fluvial response to the PETM. We show that channel-body and story thicknesses across the PETM are not statistically

significantly different from deposits outside the climate event, implying that there is not a consistent sedimentary response to the climate event across the basin. Based on our large dataset we calculate that precipitation would have had to double for statistically significant changes in deposit thickness to be generated. We discuss how climatic signals may be lost due to the self-organization, spatial-temporal varied response and preservation potential in large fluvial systems. This study gives a new quantified perspective to climate events in the geologic record.

INTRODUCTION

Earth's present-day climate is undergoing anthropogenically induced warming, with increased temperatures and storm intensities, sea-level rises, and aridification observed and predicted across the globe (IPCC 2021, 2022). Understanding how rivers and their associated floodplains respond to climate change is critical because these environments are important biogeochemical interfaces, habitats for wildlife, conduits for delivering sediment and water to the world's oceans, as well as being areas for cultivation and habitation for humans. Climate unequivocally influences the nature of river channels and their associated floodplains. Climate provides a first-order control on the amount of water present in a fluvial system as well as influencing discharge regimes (e.g., perennial, seasonal, intermittent, and ephemeral). In addition, climate influences the rate of soil development, the type and density of vegetation present on channel bars and banks and in floodplain environments, which in turn directly impacts the caliber and sediment load present in a fluvial system by influencing, in conjunction with local geology, the erodibility of the landscape and thus sediment supply into a river system. In addition, other factors, such as slope (ultimately controlled by tectonics) and base level (e.g., sea level/lake level) will contribute towards defining the dimensions, morphology (e.g., braided, meandering, anastomosing, and straight as end members), and sediment load of a fluvial system.

If all factors are kept in a steady state, a river will inherently adjust to reach equilibrium (i.e., the graded profile; Mackin, 1948). However, alluvial systems that are not undergoing transient response, for example to base-level fall, are more likely to exist in a state of dynamic equilibrium with forcing conditions that themselves are constantly changing (e.g., Bull, 1991; Dade and Friend, 1998; Whipple, 2001; Blum, 2008; Macklin et al. 2012). Defining dynamic equilibrium may also be problematic due to the multitude of autocyclic and allocyclic factors involved, which operate at different timescales and have differing response rates dependent on fluvial-system size, and the tendency of fluvial system to act in a hierarchal manner (i.e., different scales of the system responding to different magnitudes of change at different rates). Disentangling this complex range of interlinked factors that operate at different time scales is challenging, particularly because timescales far exceed the length of human observation (Toby et al., 2022). However, with careful observations and consideration of all factors involved, deductions can be made as to how, and why, rivers respond to different external forcing mechanisms. A change in climate will affect river discharge and sediment load through changes in precipitation, weathering, and vegetation dynamics. Changes in hydrological forcing cause fluvial morphological responses, including changes in channel and bar dimensions and migration rates, planform, bed sediment size, and net sediment flux, leading to aggradation (storage) or degradation (removal) (e.g., Bull, 1991; Knighton 1998; Blum and Törnqvist 2000; Macklin et al. 2012). The timescales of these adjustments to new climatic conditions depend on the magnitude and rate of changes in the forcing factors and the sensitivity of the system to change (Blum, 2008). There are a multitude of examples are available of fluvial response to changes in climate. For example, morphological changes in rivers in SE Australia have been linked to variations in flow regime consequent on Late Quaternary climatic changes (Nanson et al., 2003). Fluvial response to climate changes has also been documented in geologically based studies. For example, Chen et al (2018), report increased channel mobility and soil denudation due to increased

discharge and regional vegetation decline related to climate change during the early phase of the Paleocene-Eocene Thermal Maximum (PETM) in the Tremp-Graus Basin (Spain).

Sedimentary deposits provide insights into how Earth systems may respond in the future to extreme climate events (Pancost 2017). During the PETM (ca.56 Ma; Zachos et al. 2003) hyperthermal-event global temperatures increased because of high atmospheric CO_2 concentrations. Sea-surface temperatures rose by 5-9°C and bottom water temperatures increased by 4-5°C over approximately 8-23 ka during the onset of the PETM, remaining high for approximately 115ka, before a 42 ka recession to pre-PETM levels (Zachos et al. 2003; 2005; McInerney and Wing 2011). The PETM is an important, and one of the closest, analogues for current global temperature increases, and although rates of global temperature change during the PETM are estimated to have been slower than are predicted for the 21st Century (Wing and Currano, 2013), the PETM provides longer term (pre-event, event, and post-event) insights into landscape response to a rapid climate change event. Although it is noted that caution must be used when studying the deposits of deep time due to preservation bias and the stratigraphic completeness of deposits (Sadler 1981; Straub et al. 2020, Toby et al., 2022), such deposits can, and do, provide important insights into landscape response to climate-change events that cannot be observed over human timescales.

The Bighorn Basin is one of the most intensively studied terrestrial PETM localities globally (e.g., Gingerich 2003; Kraus and Riggins 2007; Rose et al. 2012; Bowen et al. 2014; Foreman, 2014; Kraus et al. 2015). To date, however, PETM deposits of the Bighorn Basin have not been placed into a wider stratigraphic, depositional systems context. For example, studies have concentrated on understanding successions in a single outcrop belt (e.g., Kraus et al., 2015), or channels have been compared with those that lie immediately above or below the PETM climate event in a specific study area of the basin (e.g. Foreman, 2014). In addition, it is important to understand whether there are any spatial variations in

recorded response to the PETM as a result of differences in location within the Bighorn Basin. As a result, the full extent of any recorded changes have not been fully evaluated in this well-studied sedimentary basin. Here we analyze the response of fluvial systems to the PETM in the Bighorn Basin through comparison of channel properties and associated deposits before, during, and after the PETM at several localities across the basin to understand 1) how different are the PETM deposits from the surrounding, wider, Paleogene stratigraphy and 2) whether there is a difference in recorded response to the event based on spatial location in a sedimentary basin. We hypothesize that, given the magnitude of reported changes in climate during the PETM, the channel deposits from within the PETM interval should be different from those both pre- and post PETM

REGIONAL SETTING AND PREVIOUS WORK

The Bighorn Basin is situated in northwestern Wyoming and south central Montana (USA) and is bounded by a number of thrust-related Laramide-age basement-cored mountain belts. These were present in the Paleogene and are still present today; namely the Beartooth Mountains to the west, the Owl Creek Mountains to the south, and the Bighorn Mountains to the east (Fig. 1). These mountain belts formed due to the breakup of the Sevier foreland basin as the tectonic regime switched from thin-skinned deformation in the Late Jurassic-Paleogene to thick-skinned deformation in the Late Cretaceous to Eocene (Snyder et al. 1976; Dickinson et al., 1988; DeCelles, 2004; Fan and Carrapa, 2014). The present-day southwestern margin of the basin is defined by the Absaroka Mountains, which are composed of the Absaroka Volcanics which formed during the mid to late Eocene and now cover early Paleocene structures (Rouse 1937; Sundell 1990). To the north, the Nye Bowler Lineament and Pryor Mountains are present but are not interpreted to have been a topographic barrier enclosing the basin (Dickinson et al.1988; Seeland 1998).

112 The Paleocene Fort Union Formation and the Eocene Willwood Formation form the Paleogene fill of the
113 Bighorn Basin (Fig. 1), which comprise deposits of alluvial-fan, fluvial-channel, floodplain, and minor
114 lacustrine environments (e.g. Van Houten 1944;Kraus 1985; Bown and Kraus1987; DeCelles et al. 1991;
115 Willis and Behrensmeyer 1995; Yuretich 1984; Kraus and Wells 1999; Owen et al. 2017, 2019). Generally,
116 within the basin there is a gradual change from dominantly gray paleosols in the Fort Union Fm to red
117 paleosols in the Willwood Fm, interpreted to record a change from predominantly humid to drier
118 conditions (Willis and Behrensmeyer 1995; Kraus etand Riggins 2007; Kraus et al. 2015). In a basin-wide
119 sedimentological study of the Fort Union and Willwood formations by Owen et al. 2017), a facies
120 analysis conducted (Table 2). They identified two main facies associations (channel and floodplain) with
121 several sub-facies associations present. In the channel-facies association, four sub-facies associations
122 were defined, namely gravelly braided stream, heterolithic dominantly braided, heterolithic dominantly
123 meandering, and fine-grained channel fill. in the floodplain facies association minor lacustrine, paleosols
124 (well-drained and poorly-drained), splay, and sheetflood sub-facies associations were identified. A
125 variety of statistical information was extracted from sedimentary-log data by Owen et al. (2019),
126 including channel presence (expressed as a percentage within each log), weighted mean grain size for
127 the channel, average and maximum channel thickness, and story thickness. These properties were
128 mapped across the basin, allowing a detailed paleogeographic model of the basin to be developed.
129 Owen et al. (2019) defined four broad, laterally sourced drainage systems, namely the Beartooth in the
130 northwest, the Absaroka to the west, the Washakie in the southwest, and the Owl Creek to the south.
131 All of these systems fed into an unconfined axial trunk system that flowed from south to north and was
132 approximately 150 km in length (Fig. 1). Welch et al. (2022) have corroborated this paleogeographic
133 model through provenance analysis and have provided further insights into the westerly source of the
134 Absaroka fluvial systems.

A variety of studies using several different proxies (e.g., leaf-margin analysis, $\delta^{18}O$ analysis of mammal teeth, analyses of pedogenic carbonate nodules) have established that the PETM in the Bighorn Basin saw increased mean annual temperature and decreased precipitation, as well as changes in vegetation type, vegetation density, and mammalian fauna (Table 1). Mean annual temperature (MAT) increased during the PETM from pre-PETM values of 15.7 ± 2.4 °C by 5°C, and then returned to pre-PETM conditions during the recovery phase of the event (e.g., Fricke et al. 1998; Wing et al. 2005; Snell et al. 2013). Mean annual precipitation (MAP) during the PETM decreased from pre-PETM values of 1200-1300 mm $year^{-1}$ by 30-40% before returning to close to prior conditions (1200 mm $year^{-1}$) after the PETM (e.g., Wing et al. 2005; Kraus and Riggins 2007; Kraus et al. 2013). Before the PETM, the landscape was dominantly forested with deciduous, evergreen, broad-leaved, and coniferous taxa. During the PETM a less dense dry tropical forest structure dominated by the bean family was present, but interestingly the plant communities returned to their previous configuration during the later stages of the PETM (Wing et al. 2005, Smith et al. 2008). In addition, dwarfing of mammalian fauna has also been recorded during the PETM (Gingerich 2003). It has been suggested that enhanced seasonality in rainfall (see Foreman, 2014) and temperature (Snell et al. 2013) occurred during the PETM.

Here we examine three outcrop belts that cover the PETM in the Bighorn Basin, two (Saddle Mountain, SM; Polecat Bench, PCB) are found within the axial system, whilst Sand Creek Divide (SCD) occurs within a small distributive system that drains from the Owl Creek Mountains (Fig. 1). Previous studies at PCB report that the paleosols become more welded (amalgamated; see Ruhe and Olson 1980) and are therefore thicker during the PETM when compared to immediately underlying pre-PETM and overlying post-PETM deposits (Kraus et al. 2015). foreman (2014) notes at SM, located in the center of the axial system (Fig 1), the presence of an uncharacteristically thick amalgamated fluvial deposit (”boundary sandstone”) within the PETM interval, with gray to red/orange paleosols located both above and below the deposit. At Sand Creek Divide (SCD), a similar situation to that at PCB is reported whereby a change

159 to drier, thicker and more mature soils is observed during the PETM interval (Kraus and Riggins 2007;
160 Rose et al. 2012).

161 Work has focused on deposits that are at, or close to, the PETM boundary at these three locations. Here
162 we present sedimentary-log data from an additional 25 sections from across the basin (see Fig. 1), giving
163 in total 12 sections from the Fort Union Formation and 16 from the Willwood Formation, together
164 allowing the deposits from the three previously studied PETM locations (Fig. 1) to be placed into a wider
165 basin context. Observations and comparisons are conducted spatially at the outcrop-belt scale and at
166 the basin scale, as well as temporally, by statistically comparing data from the PETM to the wider
167 Paleogene fill within a newly defined paleogeographic depositional system context (Owen et al. 2019).
168 This approach allows the PETM sections to be considered within a basin-scale, depositional-system
169 context, therefore allowing full assessment of fluvial response to a hyperthermal event, including an
170 evaluation of the degree of variability in the response at a range of scales (e.g., outcrop to basin scale).

171 **METHODS**

172 This paper builds on the work of Owen et al. (2019) but differs by focusing specifically on the
173 sedimentological characteristics of floodplain and channel deposits pre-, during, and post- PETM.
174 Sedimentary-log data were collected at 50 mm resolution at 28 locations across the basin (Fig. 1),
175 totaling 4,192 m of stratigraphy (see Appendix 1 for sedimentary log-data). Facies association and
176 channel-body geometries were defined from sedimentary and architectural data based on the scheme
177 of Owen et al. (2017; see Table 2). Here, a channel body is defined as being the three-dimensional form
178 that is deposited from processes operative within channels (see Gibling 2006 for discussion). A channel
179 body is encompassed by floodplain deposits and may be a single story or may comprise complex
180 amalgamated deposits. Channel bodies have in previous studies been used to infer a fluvial stratigraphic
181 response to the PETM (e.g. Schmitz and Pujalte, 2003;oreman 2014;; Chen et al. 2018). By studying

channel-body characteristics, insights into controlling variables (e.g., accommodation versus sediment supply linked to climate and tectonics, migration rate, planform, and deposition/erosion rates; Bridge 1993) can be gained. We define a story surface as being the "*erosional elements of the active portion of a channel base, which incise into previous channel deposits*" *sensu* Owen et al. (2017). By measuring the story thicknesses, we are able to understand how incision rates, which relate directly to channel depth and discharge, vary throughout the basin.

The thickness of channel bodies was measured vertically where exposure permitted. Channel-body widths and story widths were not measured, as larger channel deposits commonly extend beyond the area of outcrop exposure and provide only a minimum estimate, and smaller channel bodies often lack complete exposure and equally would not provide an accurate value. Story surfaces often crosscut one another and thus do not fully represent the true widths of the channel. As a result, and to provide a consistent method for comparison, we utilize only thickness data in this study. This dataset was analyzed in its entirety where pre-PETM, PETM, and post-PETM channel data were compared. Data from the axial system alone were then analyzed separately to compare pre-PETM, PETM, and post-PETM) deposits from the same system. Data from exposures in a transect across the axial system, perpendicular to flow, were then used to understand lateral variation at approximately the same position downstream in a single system (pre-PETM, PETM, and post-PETM); see Fig. 1 for locations.

Where data were available, a mammalian age group was assigned (Paleocene, undiff; Tiffanian; Clarkforkian; Wasatchian-1 to Wasatchian-4; Wasatchian-5 to Wasatchian-7) to each of the sedimentary logs based on the work of Gingerich and Clyde (2001), allowing an approximate biostratigraphic framework to be established for the sedimentary logs. Isotopic curves that indicate the start of the PETM and sedimentary log data were utilized from previously published datasets (Kraus and Riggins 2007; Foreman 2014; Kraus et al. 2015) to pinpoint the location of the PETM.

RESULTS

SEDIMENTARY OBSERVATIONS OF PETM SECTIONS

Sedimentary logs and example images for the three studied PETM outcrop belts in the Bighorn Basin, shown in Figures 2, 3, and 4, show considerable differences. At Sand Creek Divide (isotopic data utilized from Rose et al., 2012) the pre-PETM section is dominated by drab gray soils and minor channel units (Fig. 2, 3A). In the Pre-PETM succession paleosols are gray, with orange to purple mottling present. They are generally moderately to well developed and rich in organic matter with leaf beds present. Interspersed between the paleosols are small-scale (up to 8 m thick) single-story channel deposits that display trough cross-bedding and accretion surfaces. Towards the top of the pre-PETM succession (base of SD-d.2 and SD-e.1; Fig. 2, 3A, B) a gradual change in the color of the soils is observed from orange to red. The red soils, which are moderate to well-formed, then start to dominate the succession during the PETM and continue to dominate in the post-PETM succession (SD-e.1; Fig. 2,3B). No channel deposits were recorded in the PETM interval at SCD. A series of logs lateral to the main PETM section (SD-e.1; Fig. 2) were measured (using isotopic data and “Red 1” of Rose et al. 2012 as a marker bed with beds being laterally traced). In log SD-e.1, the onset of the PETM shows a gradual transition in the occurrence and maturity of the red soils. SD-d.2, however, does not show any indication of a change in the nature of the soils at the start of the PETM and continues to be dominated by gray soils with purple and orange mottling present well into the PETM (Fig. 2). Interestingly, farther up the vertical section, lateral changes are also visible. At the onset of the PETM recovery, SD-e1 shows a thick, very mature paleosol (“big red”; Fig 2. 3B), However, laterally this soil is considerably thinner (SD-e.2) but still forms a mature soil dominated by red and purple mottling. In addition, in SCD1, a thick (10 m), multistory channel is observed lateral to and slightly above, ‘big red’ (i.e. the bed above; logSD-f-Fig 2) whereas laterally (SD-e.2) floodplain deposits dominate, with only moderate gray paleosol development indicating wetter

conditions. Therefore, a large degree of variability is present in the PETM deposits in the SCD outcrop belt. Similar observations have been made by Kraus and Riggins (2007) in the same outcrop belt, noting a change to more welded (amalgamated), thicker and drier soils during the PETM, but that the red well-drained B horizon vertic paleosols do grade laterally into poorly drained gray paleosols that are interpreted to be Bssg horizons of Vertisols.

At Polecat Bench only a small part of the pre-PETM succession is exposed and the succession is dominated by gray, poorly formed paleosols with orange mottling (Fig. 4A). However, close to the PETM onset (approximately 8.5 m PCB log; Fig. 4A) well-developed red soils begin to gradually appear and then dominate the lower part of the PETM succession. From ~25 m in the section and upwards, channel deposits appear within the PETM succession. Channel deposits in the PETM are dominated by lower-flow-regime structures such as trough cross-bedding and ripples, which are composed only of moderately sorted sandstone with very coarse sand to granule-grade material present on some cross-sets. The channel deposits become thicker and more frequent up-section, but, the exact location of the recovery period is inferred at this specific location due to channel erosion, with the final channel deposit proposed to be above the PETM interval (Gingerich 2001). In between the channel deposits the paleosols continue to be red, mature, and well-formed with carbonate nodules, mottling, and root structures present. Other studies at the Polecat Bench outcrop belt have noted similar trends where a change to more welded, thicker and drier soils is observed during the PETM (Kraus et al. 2015). In addition, a sedimentary log has been constructed from a core that was retrieved from behind (approximately100m) the outcrop exposure (Fig. 2 of Kraus et al. 2015). The authors noted in the core, a change to more mature, more welded soils is observed during the PETM succession, and that channel and related splay deposits are more abundant in the core compared to sedimentary logs taken at the outcrop. We observe similar channel and related splay deposits in our sedimentary log (e.g., approximately 35 m, Fig. 4A). Thus, although similarities can be observed between the three logs, such

as the dominance of red mature paleosols over other types of paleosols, there is inherent variability in the presence of channel deposits in the PETM interval at the Polecat Bench outcrop belt. A key difference between our logs and those previously published, however, is that we observe one relatively thick (4 m) channel in our log (~=approximately 26 m, Fig. 4A).

A noticeable change in the nature of the PETM succession is observed at the Saddle Mountain outcrop belt, which is situated in the middle of the basin in the axial system. The base of the recorded succession (below the PETM) is dominated by a 17-m-thick multistory (three stories) channel body with lower-flow-regime structures present (trough cross-bedding and ripples) (Fig. 3C, 4B). The succession above this is then dominated by floodplain deposits which are composed predominantly of gray soils with orange and purple mottling that become increasingly redder towards the top of the pre-PETM succession. In the PETM interval the base is dominated by floodplain deposits composed of red paleosols and splay deposits; however, a large, internally amalgamated channel body appears from approximately 60-84 m on the log. The channel body is thick (24 m), is composed of four stories with accretion surfaces, with trough cross-bedding and planar to low-angle planar lamination present (Fig. 3). Wood debris, carbonate nodules, and coarser grained material commonly line cross sets. Separating the storys are thin (up to 4 m) packages of green to gray mud and fine sandstone sheets within which carbonate nodules, woody debris and plant material can be observed. Above the channel body a thick (9 m) floodplain package is present which is dominantly gray and contains one mature red paleosol with rootlets and carbonate nodules present. An additional channel body was observed in the outcrop during the PETM recovery onset that is thinner (10 m) than the channel observed in the PETM proper but is very similar sedimentologically. However, this channel body has a slightly different geometry in that it has an offset stacked pattern (Fig.4). Foreman (2014) also documented the presence of a large channel body (the ”boundary sandstone”) within the PETM interval. He noted that the boundary sandstone varies in thickness across the outcrop belt as well as displaying variations in stacking arrangement and the

presence of mud in the channel body and between story surfaces. These observations, again, highlight the variability observed in PETM successions in single outcrop belts.

In summary, the field observations from each of the three outcrop belts highlight that there is a considerable variability in fluvial facies characteristics both in single outcrop belts and between the different outcrop belts across the basin when looking at deposits within, and immediately above, and, below the PETM. These observations raise the question as to whether it is possible to identify a consistent, contemporaneous environmental change within the PETM across the basin given the variations observed in each of the logged sections, given the magnitude of change in precipitation and temperatures that has been reported to occur in the basin.

STATISTICAL ANALYSIS

To assess the impact of climate change on the fluvial system, PETM channel bodies (N = 3) are compared with those from the pre- (n = 109) and post-(n=73) PETM successions. This small sample size for PETM channels reflects the paucity of channel bodies in this part of the basin rather than sampling bias (see Appendix for logs of entire basin and Paleogeography of Owen et al. 2019), particularly in documented PETM intervals. However, whilst this is a small sample size, it is compared to much larger datasets from the pre- and post-PETM stratigraphy. The mean channel-body thickness of the PETM channel bodies (12.40 ± 5.9 m; cv = (standard deviation/mean) = 0.82; N = 3) exceeds both pre- (7.49 ± 0.69 m; cv = 0.96; N = 109) and post- (7.66±0.78 m; cv = 0.87; N=73) PETM values for the whole basin. When considering just the axial system (where PETM channel bodies are found), the pre-PETM average thickness (7.65 ± 0.77 m; cv = 0.53, N = 28) and post-PETM average thickness (7.19 ± 0.64m; cv = 0.49; N = 30) are both smaller than PETM values (12.40 ± 5.9 m; cv = 0.82; N = 3). When considering just a transect through the northern part of the axial system (i.e., channel deposits at the same position

downstream in the axial system) PETM channel bodies are on average larger than those pre-PETM (7.75 ± 0.88 m; cv = 0.56; N = 24) and post- (8.25±0.93 m; cv = 0.39; N = 12) PETM.

The coefficients of variation for the whole-basin dataset are greater than for the whole axial (pre-PETM 0.53; post-PETM 0.49) and northern axial (pre-PETM 0.56; post-PETM 0.39) transects. None of the differences above (whole basin, Northern axial, axial) in mean channel-body thickness (pre-, during, and post-PETM) are statistically significant (ANOVA; p-values = 0.33 whole basin data (log transformed); 0.27 Northern axial, 0.13 axial).

PETM channel-body thicknesses lie within the range of measured channels from the Paleogene fill (Fig. 5A), with the average PETM measurement falling within the range (mean ± 1 standard deviation) of all datasets analyzed. Indeed, the measured channel thicknesses for the PETM are not the largest in the basin (Fig. 6), with channel measurements from Foreman (2014) for the PETM also lying within the range of measured channel body thicknesses in our basin-wide dataset.

However, the story (channel depth) thickness dataset shows different results. The mean story thickness of the PETM channel bodies (4.65 ± 0.98 m; cv 0.59; N = 8) is very similar to the pre-PETM (4.67 ± 0.27 m; cv = 0.73; N = 154) and post-PETM (4.67 ± 0.22 m; cv = 0.47; N = 101) values for the whole basin. When considering just the axial system, the pre-PETM average story thickness (4.29 ± 0.24 m; cv = 0.39, N = 50) and post-PETM average thickness (4.49 ± 0.29 m; cv = 0.44; N = 48) are only slightly smaller than PETM values (4.65 ± 0.98 m; cv = 0.59; N = 8). For the northern transect across the axial system (See Fig. 1 for location) PETM channels are again only slightly larger than pre-PETM (4.54 ± 0.27 m; cv = 0.38; N = 41) and post-PETM (4.30 ± 0.31 m; cv = 0.35; N = 23) values.

Story thicknesses for the PETM interval are within the range of all other datasets (e.g., pre- and post-PETM) Fig. 5B) with the exception of the post-PETM northern transect dataset where the range in story

thicknesses is smaller. However, the average story thickness of the post-PETM northern transect still lies within the range of measured story thicknesses for this dataset. In all but the pre-PETM basin-wide dataset, the coefficient of variation is larger for PETM deposits than either pre- or post-PETM deposits, which is to be expected due to the smaller sample size for the PETM. The lack of any significant change in channel depth indicated by the story thickness suggests that the axial fluvial system did not undergo significant change in morphology or size through the PETM period. The channel body data support this; although the three PETM channel bodies are on average thicker than both pre- and post PETM, this is not a statistically significant difference. As was the case for the channel-body deposits, none of the differences in mean story thickness (pre-, during, and post-PETM) are statistically significant (ANOVA; p-values = 0.48 whole basin data (log transformed); 0.85 Northern axial; 0.81 axial).

DISCUSSION

EXPECTED STRATIGRAPHIC RESPONSE TO CLIMATE CHANGE

The analysis of measured channel-body and story thicknesses shows significant variability within each time interval and, although mean values do show some differences within the PETM, these are not statistically significant given the high degree of observed variability. To further assess the significance of these results, we consider the potential stratigraphic response of the Bighorn Basin axial fluvial system to the PETM by calculating expected channel size based on the 30% reduction in precipitation that has been estimated to occur from pre-PETM to the PETM (e.g. Wing et al. 2005; Kraus and Riggins 2007; Kraus et al. 2013) (Table 4). However, this reduction in mean precipitation is likely to have been accompanied by increased seasonality such that formative discharge events may have increased in magnitude during the PETM (Foreman, 2014) so causing increase in story thickness. The statistical analysis is restricted to the axial system to avoid bias imparted by the different size lateral systems present along the basin margins. Using values for the mean, standard deviation and sample size (N)

reported above, we calculate the increase in mean story thickness required during the PETM for this to be statistically significant (using a t-test to compare pre-PETM and PETM values). Note that the small (N = 8) number of PETM values leads to a relatively high standard deviation for this interval, which results in high story-thickness increases being required in order to be statistically significant. To account for the sample-size effect on estimated standard deviation, a further calculation was made using the lower pre-PETM standard deviations as an indication of natural variability in the deposits. This approach suggests conservative (lower) increases in thickness necessary to be statistically significant.

To represent a statistically significant increase, the minimum PETM average story thickness in the northern axial transect would be 5.80 m (Table 4), (+ 1.27 m pre-PETM mean and +1.15 m higher than the PETM mean). The significant story thickness rises to 6.46 m using the standard deviation from the eight PETM measurements. For the whole axial system, the significant mean thickness would be 5.49 m (+1.21 m of pre-PETM and +0.85 m than PETM mean; Table 4). Again, using the measured standard deviation estimate increases the significant mean value, here to 6.19 m.

The statistically significant changes in channel depth (story thickness) can be used to estimate the increase in discharge (Q) that would be required to produce channel adjustments of this magnitude. We used a hydraulic-geometry relationship (Leopold and Maddock, 1953)

$$h = cQ^f$$

where h is flow depth [m], and c and f are empirical constants. The exponent f is taken as 0.4, based on extensive global data (Knighton, 1998). To generate statistically significant depth changes for a single channel located along the northern axial transect, Q needs to increase by a factor of 2.42 using story thickness calculated with the standard deviation from the PETM data (N = 8) (Table 2). For the axial system dataset a similar magnitude of increase is suggested (2.51; Table 2). These results show that a

365 statistically significant stratigraphic response requires increased discharge, and therefore storm-event
366 runoff (Knighton 1998) during the PETM to more than double compared to pre-PETM values. Such an
367 increase in discharge, which could be related to increased storm-event precipitation and runoff from
368 sparsely vegetated hillslopes, is opposite to estimates (30% decrease) of mean annual precipitation
369 changes from pre-PETM to the PETM (Table 1).

370 Increasing seasonality of precipitation and river discharge could lead to channel-geometry adjustments
371 (Knighton 1998), and more variable flow will also affect the nature of deposits (e.g., Fielding et al. 2009;
372 Plink-Björklund 2015). Potentially enhanced seasonality in rainfall (Foreman, 2014) and temperature
373 (Snell et al. 2013) during the PETM could have resulted in increased storm-event precipitation while
374 overall precipitation decreased. However, recent modelling indicates complex atmospheric behavior in
375 the Bighorn Basin and suggests a reduction in extreme precipitation rates, although when high CO_2
376 levels are modelled an increase in the rarest precipitation events may have occurred more often
377 (Carmichael et al. 2018). Carmichael et al. (2018) note that although these inferred responses are
378 contradictory, precipitation events in the area are broadly regular and of low intensity. Grain-size
379 datasets for channels (Owen et al. 2019) show that the PETM channel sediments (average 0.27 mm) lie
380 in the range of those within the northern axial transect (average 0.21 - 0.47 mm) implying no significant
381 change in river bed sediment size during the PETM. Story surface depths do not change significantly, and
382 there is little change in the sedimentology of the channels, with bedforms remaining similar to those in
383 both pre- and post-PETM deposits (Foreman, 2014). The internal sedimentology of the fluvial channels
384 therefore suggests that enhanced seasonality, if present, had little effect on the resultant preserved
385 channel-deposit characteristics. This is not wholly surprising given the axial river location as most of the
386 coarsest material is trapped upstream in the proximal part of the basin, in basin-margin-transverse
387 systems.

389 A change in climate, causing changes in river discharge and sediment loads, will result in geomorphic
390 and sedimentological changes, the magnitude of which will depend on the nature of the river system
391 and its sensitivity to change. Thus, fluvial sediments deposited during a climate event may be different
392 from those before the event. For the environmental changes that resulted from the PETM in the Bighorn
393 Basin to be recorded in the three studied PETM outcrop belts, the response of the fluvial system to
394 these changes would need to be propagated from the source catchments through multiple transverse
395 systems that supplied the axial system in the basin. Regionally, river systems can respond synchronously
396 to climatic changes (e.g., Bull 1991; Macklin et al. 2002), but more frequently they respond at different
397 rates and times (e.g., Starkel 1991; Slater and Singer 2013). Whether responses are regionally consistent
398 depends on the magnitude and rate of forcing, with larger, faster changes in environmental conditions
399 being more likely to result in synchronous and consistent responses. If all catchments in the Bighorn
400 Basin responded synchronously to the PETM, the signal in the axial system should be amplified.
401 However, if the lateral systems responded at different times and rates, a dampened and extended signal
402 of the climate event would be expected in the axial system. The latter scenario is expected because the
403 lateral river systems are of differing sizes and will respond at different rates to external perturbations
404 (Blum 2008). Hence a muted signal is hypothesized to reach the distal reaches (e.g. Saddle Mountain,
405 Fig. 1) of the axial system. Numerical models demonstrate that rivers can attenuate or absorb external
406 signals through internal system dynamics (e.g., avulsion, sediment storage and release), and suggest
407 that significant geomorphic thresholds (e.g., critical slope; Schumm 1979) need to be met for
408 environmental signals to be recorded (e.g., Jerolmack and Paola 2010; Straub et al. 2020). Indeed,
409 recent work by Ganti et al. (2020) using theoretical and field-based studies suggests that the
410 stratigraphic record captures ordinary events ("*Strange ordinariness*", Paola et al. 2018) due to the
411 inherent manner in which fluvial systems self-organize. Ganti et al. (2020) showed from modelling that

412 higher sedimentation rates should lead to higher preservation potential of bar deposits during the PETM
413 (compared to pre- and post-PETM); however, if higher sedimentation rates led to increased avulsion and
414 migration rates, then preservation of extreme conditions would be consistent across pre-PETM, PETM,
415 and post-PETM strata. Our sedimentological observations (e.g., grain size, cross-set height, and story
416 height) from strata during and across the Paleocene and Eocene support the latter conclusions drawn by
417 Ganti et al. (2020). These combined factors result in a low likelihood of a short-term signal being
418 preserved within the geologic record.

419 A more amalgamated body ("boundary sandstone") is present at Saddle Mountain during the PETM
420 (Figs. 3C, Fig 4; Foreman, 2014); however, the boundary sandstone is not consistently thick (Foreman,
421 2014) nor is it anomalous with respect to its stacking geometry when compared to other sandbodies in
422 this area (i.e., axial fluvial system, northern transect) of the basin (e.g., Fig.7B; Owen et al. 2017). It is
423 argued by Foreman (2014) that the boundary sandstone resulted either from deposition induced by
424 adjustment of river gradient to changes in supply of sediment and water, or from decreased bank
425 stability due to a decrease in vegetation cover. Modelling of the former (Simpson and Castelltort 2012)
426 shows that a significant distal response is expected only once wetter conditions with higher transport
427 capacities return. Hence, because of the inference of a decrease in mean annual precipitation during the
428 PETM (Table 1), any change in channel form should be observed either in the later PETM or early post-
429 PETM deposits after a return to pre-PETM precipitation values, particularly because a lag time of 14-25
430 ky is to be expected in the Bighorn Basin (Duller et al. 2019). Our data do not support the alternative
431 scenario of decreased bank stability, inasmuch as a shallowing and change in planform are not observed,
432 which would be expected if bank stability decreased as rivers would widen. In addition, other published
433 PETM sedimentary logs show that more welded and/or amalgamated soils can be present (although
434 laterally variable) such as those seen at Polecat Bench (Kraus et al. 2015), implying that a more
435 structured and cohesive floodplain was present, which would in turn result in an increase in bank

436 stability. Given the boundary sandstones variable thickness in the depocenter of the basin, we
437 hypothesize that autogenic processes such as avulsion have driven the formation of a larger sandstone
438 body at SM where the axial system is present. A thicker sand body may therefore be a local expression
439 of internal system dynamics rather than indicating a response to external drivers (Jones and Hajek
440 2007).

441 The preservation of autocyclic processes over allocyclic processes in the stratigraphy of the Bighorn
442 Basin fluvial systems is not unexpected when considering the paleogeography of the basin. The fluvial
443 systems that entered the Bighorn Basin were supplied from different catchments of variable sizes (Fig. 1;
444 Owen et al. 2019). The Absaroka and Washakie catchments fed and resulted in large, coarse-grained
445 fluvial systems sourced from outside the immediate basin area. In contrast, the Beartooth and Bighorn
446 mountains are considered to have been source areas for locally derived alluvial and fluvial fans, with the
447 Owl Creek catchment to the south supplying relatively small-scale fluvial systems to the basinal area
448 (Owen et al. 2019). Of the studied sections, Sand Creek Divide was supplied solely from the Owl Creek
449 catchment, whereas Polecat Bench and Saddle Mountain are both located within the axial fluvial system
450 (Fig. 1). Thus, Sand Creek Divide will record only a climatic response from the Owl Creek drainage,
451 whereas Saddle Mountain and Polecat Bench will record an amalgamation of climate responses from
452 immediately adjacent alluvial and fluvial fans, the Owl Creek, Washakie, and Absaroka catchments. It is
453 expected that these catchments will respond over different time scales to any climatically induced
454 perturbation depending on elevation, gradient, size, grain-size availability, bedrock lithology, and
455 downstream distance to the logged sections (Duller et al. 2019). Thus, any allocyclic climate signal in an
456 axial fluvial system is likely to be shredded by a combination of different lag times in different-sized
457 catchments as well as ongoing autocyclic processes such as avulsion. Further modelling work is needed
458 to quantitatively explore how having multiple, and different sized, pathways in a source-to-sink system
459 will affect the expected signal propagation and resultant stratigraphy, particularly with regard to

460 preservation in axial systems. A record of a global climate signal in a fluvial system is more likely to be
461 preserved if the fluvial system is sourced either from a single catchment area with a uniform climate, or
462 where immediately adjacent catchments respond to the same climate event, such as in a bajada-type
463 setting (e.g., Cesta and Ward, 2016).

464 When analyzing the effects of climate on fluvial systems, it is imperative that other factors, such as
465 tectonics and baselevel, have been accounted for (Vandenberghe, 2002, Macklin et al. 2012). The role of
466 tectonics in the Bighorn Basin has largely been disregarded (Foreman 2014); however, our basin-wide
467 study shows evidence of tectonic processes (Fig. 7A). The assumption that there was a lack of tectonic
468 activity during the PETM cannot be made, because there are unconformities present that span the
469 Paleocene-Eocene, providing evidence for tectonic activity around the basin margin (Fig. 7A). Thus, with
470 syntectonic activity it is expected that subtle increases and decrease in accommodation, along with
471 sediment-supply variations due to uplift and/or exposure, and changes in channel amalgamation rates
472 could be another way in which thicker deposits can be formed, particularly in axial systems (e.g., Connell
473 et al. 2012). Variable subsidence rates have been found across the basin (Clyde et al., 2007), with slow
474 rates of subsidence in the SE (Owl Creek systems, approximately 85 m/Myr.) but high rates in other
475 areas such as McCullough Peaks (approximately 250 m/Myr) and Polecat Bench (approximately 200
476 m/Myr) both situated in the axial part of the basin.

477 Prior comparisons of the sedimentology of the PETM successions have been made only during the PETM
478 and immediately before and after the PETM event (e.g., Kraus et al. 2015; Foreman 2014). Cyclicity, i.e.,
479 repeated channel and floodplain deposition, is evident in the basin fill, and is an order of magnitude
480 larger than the discussed study intervals for the PETM. Channel bodies have a return thickness of
481 approximately 20-30 m in the axial system (see Fig. 7C for example), whereby the top of one channel
482 body is separated by approximately 20-30 m of floodplain deposits before the base of the next

483 sandbody is encountered. Although the PETM spans only a single channel-body avulsion package, it is
484 essential that the deposits are discussed within the context of the overall system dynamics, which, in the
485 case of the Bighorn Basin, requires the study of channel-body deposits 20-30 m above and below in
486 order for an assessment for any significant changes to be made. Our basin-scale dataset considers the
487 gross-depositional fill of the basin by studying the deposits substantially below and above those of the
488 PETM. In addition, mature, red paleosols are not unique to the PETM. In the basin fill, multiple mature,
489 red paleosols are present below, but more commonly above, the PETM in both the axial (Fig. 7C) as well
490 as the surrounding lateral systems (e.g., Kraus and Wells, 1999; Kraus, 2001; Abels et al. 2013. This
491 implies that the paleosols are either not unique to this particular climate event and can be formed
492 through other mechanisms (e.g., areas of the floodplain that are dry due to a position distal to a
493 channel) or that to generate such paleosols there is a need for other climate events that have not, as
494 yet, been identified in the basin fill.

495 We stress that we are not implying that river dynamics and deposits may not respond to climatic
496 changes, but that the stratigraphic signature is negligible, or signal-to-noise (i.e., autocylcic processes) is
497 too low to be detectable in the Bighorn Basin when placed into a wider stratigraphic and systems
498 context. In much more climatically sensitive areas, a similar degree of climate change could have more
499 significant consequences. Our results suggest that in this particular climate zone the magnitude and rate
500 of environmental changes associated with the PETM are insufficient to overcome geomorphic
501 thresholds controlling channel pattern and size and so are not recorded in a statistically significant way
502 in the geological record in the axial and Owl Creek systems. We fully recognize that channel-body
503 deposits, at the extreme end of the data, are thicker than those of similar deposits (e.g., in the axial
504 fluvial system); however, this channel body is not uniformly thick across the axial system with the
505 average thickness of the channel body sitting within the “norm” of channel deposits. In addition,
506 sedimentary-log data from other localities show that there is considerable variation laterally even at the

outcrop-belt (several kilometers) scale, as is observed by the variable thickness of channel and splay deposits in the "boundary sandstone interval" at Polecat Bench and Saddle Mountain (Fig. 4) and the nature of paleosols deposits at Sand Creek Divide (Figs. 2, 3). Such variability is to be expected across a landscape dominated by fluvial systems as environments transition from one to another (e.g., fluvial channel to proximal to distal floodplain) with local hydrological conditions, vegetation and topography influencing characteristics at a local and basin scale. However, our study follows the principles of Walther's Law (Middleton, 1973) and highlights that when studying the influence of events, such as climatic fluctuations on systems, it is imperative that natural landscape variability (i.e., spatial variability) is taken into consideration, as different interpretations of the effect of events may differ depending on where log locations are taken on the relict landscape. Indeed, recent work by Dzombak et al. (2021) demonstrated variability in paleosol proxy work along an extensive outcrop belt in the Green River Basin, SW Wyoming. This work highlights that there is inherent uncertainty when using proxies from single sections to infer basin-scale trends and that it is important to understand the true variability that can be present.

CONCLUSIONS

Our study provides a unique framework for analyzing climatic events in the terrestrial rock record by highlighting the importance of considering sedimentary signatures interpreted to be generated by climate change within a wider stratigraphic and depositional systems context. Our results indicate that sedimentary patterns during the PETM are not consistent across single outcrop belts in the Bighorn Basin, let alone across the entire basin, with river behavior during the PETM being within the normal range found in the rest of the basin fill. This result is not wholly unexpected given Walther's Law, but it highlights the importance of studying climate events with appropriate contextual data. Our results suggest that the PETM climatic perturbation was not of sufficient duration or magnitude to generate a

statistically significant fluvial stratigraphic response in the axial or Owl Creek systems of the Bighorn Basin. Our calculations from a single channel show that a significant (more than double pre-PETM levels) increase in storm-event precipitation would be required for a clear stratigraphic response. This study has important wider implications for how we understand the spatial variability in environmental response to climate events and how we appropriately utilize the stratigraphic record to project future climatic response.

ACKNOWLEDGMENTS

AO, AH, and GW thanks FSRG 2 sponsors for funding field campaigns. AE thanks University of Aberdeen for funding field work. We thank all residents in the Bighorn Basin who allowed access to private land to study the Paleogene fill, which greatly enhanced the size and quality of this dataset. Isobel Buchanon, Alistair Swan, and Mauricio Santos are thanked for their assistance in the field.

FIGURE CAPTIONS

Figure 1 A) Paleogeography of the Bighorn Basin during the Paleogene and localities studied. Modified from Owen et al. (2019). Please see Appendix 1 for sedimentary logs of locations. B) Generalized stratigraphic column of the study area.

Figure 2. Sedimentary logs taken across the Sand Creek Divide outcrop belt. Location of PETM (i.e. isotopic data), ”Big Red” and ”Red 1” taken from Rose et al. (2012).

Figure 3. Example images of the PETM. A) Image of log location at SD-d1 and d2 at Sand Creek Divide. Note that this log is lateral to the image in part B. B) Image of log SD-e1. Note the persistence of red soils that laterally turn gray in part A. C) Boundary sandstone at Saddle Mountain. Note the presence of

551 mudstone packages in the boundary sandstone that clearly separate stories in the channel body. Please
552 see Figure 4, or Appendix 1, for sedimentary log detail

553 Figure 4. A) Sedimentary logs of Polecat Bench. PETM location in the stratigraphy taken from Kraus et al.
554 (2015). B) Sedimentary log of Saddle Mountain. PETM location in the stratigraphy is taken from Foreman
555 (2014).

556 Figure 5. Box and whisker plots summarizing the measured data. A) Channel-body thickness and B) story
557 thickness. In this study story surfaces are considered to represent channel depth as they scale to bar
558 clinoform height (and therefore flow depth).

559 Figure 6. Histogram data for all channel bodies in the Bighorn Basin. Note that PETM channel-body
560 thicknesses are highlighted with stars (this study) and those recorded in other studies (arrows).

561 Figure 7. A) Angular unconformity in the SW part of the basin. Note dipping, interbedded channel and
562 floodplain deposits of the Fort Union (Paleocene) and flat-lying conglomeratic units of the Willwood
563 (Eocene) deposits. B) Photopanel of axial fluvial deposits in the western area of the northern transect of
564 the axial fluvial system. Note the occurrence of thick sandstone bodies that occur every 20-30 m in the
565 basin fill stratigraphy. C) McCullough peaks exposure highlighting the persistence of thick red soils
566 elsewhere in the stratigraphy.

567 **TABLE CAPTIONS**

568 Table 1. Summary of key characteristics pre-PETM, PETM, and post-PETM in the Bighorn Basin.

569 Table 2. Summary descriptions of facies associations observed in the Paleocene and Eocene fill of the
570 Bighorn Basin (see Owen et al., 2017, for full descriptions of facies and geometries).

Table 3. Summary data (in meters) for channel-body and story deposits pre-PETM, PETM, and post-PETM for the whole basin, whole axial system, and northern basin transect. See Figure 5 for graphical representation of dataset.

Table 4 - Summary statistical results comparing pre-PETM and PETM channel depths (story thicknesses). Results are presented for two assumptions for standard deviations, s.d., for the PETM data: (1) s.d. calculated from all eight available measurements; (2) s.d. estimated as being the same as in the larger pre-PETM data sets for the same locations. The estimates of channel-forming dischargewere calculated using $f = 0.4$ in an empirical relationship between channel depth, h, and discharge, Q, $h = cQ^f$.

APPENDIX

The appendix contains five sections, each of which shows the summarized raw sedimentary logs for all locations studies. Section A1.1: Sedimentary logs from the Beartooth systems. Section A1.2: Sedimentary logs from the Absoraka systems. Section A1.3: sedimentary logs from Washakie sedimentary systems. Section A1.4: sedimentary logs from the Owl Creek systems. Section A1.5: sedimentary logs from the Axial system.

REFERENCES

Abels, H.A., Kraus, M.J., and Gingerich, P.D., 2013, Precession-scale cyclicity in the fluvial lower Eocene Willwood Formation of the Bighorn Basin, Wyoming (USA): Sedimentology, v. 60, p. 1467-1483.

Blum, M.D., 2008, Large River Systems and Climate Change, *in* Gupta, A. ed., Large Rivers: Geomorphology and Management: John Wiley & Sons, p. 627–659.

591 Blum, M.D., and Törnqvist, T.E., 2000, Fluvial responses to climate and sea-level change: a review and
592 look forward: Sedimentology, v. 47, p. 2–48.

593 Bowen, G.J., Maibauer, B.J., Kraus, M.J., Röhl, U., Westerhold., T., Steimke, A., Gingerich, P.D., Wing,
594 S.L., Clyde, W.C. 2014 Two massive, rapid releases of carbon during the onset of the
595 Palaeoecene-Eocene thermal maximum: Nature Geoscience, v. 8, p. 44-47.

596 Bown, T.M., and Kraus, M.J., 1987, Integration of channel and floodplain suites, developmental
597 sequence and lateral relations of alluvial paleosols: Journal of Sedimentary Petrology, v. 57, p.
598 587–601.

599 Bull, W.B., 1991, Geomorphic Responses to Climate Change: Oxford, Oxford University Press, 326.p.

600 Bridge, J.S., 1993, Description and interpretation of fluvial deposits: a critical perspective:
601 Sedimentology, v. 40, p. 801–810.

602 Carmichael, M.J., Pancost, R.D., and Lunt, D.J., 2018, Changes in the occurrence of extreme
603 precipitation events at the Paleocene–Eocene thermal maximum: Earth and Planetary Science
604 Letters, v. 501, p. 24–36.

605 Cesta, J.M., and Ward, D.J., 2016, Timing and nature of alluvial fan development along the Chajnantor
606 Plateau, northern Chile: Geomorphology, v. 273, p. 412-427.

607 Chen, C., Guerit, L., Foreman, B.Z., Hassenruck-Gudipati, H.J., Adatte, T., Honegger, L. Perret, M.,
608 Slujis, A., and Castelltort, S., 2018, Estimating regional flood discharge during Palaeocene-
609 Eocene global warming: Scientific Reports, v. 8, P. 1-8.

Clyde, W.C., Hamzi, W., Wing, S.L., Schankler, D., Chew, A., 2007, Basin-wide magnetostratigraphic framework for the Bighorn Basin, Wyoming: Geological Society America Bulletin, V.119, p. 848-859.

Connell, S.D., Wonsuck, K., Paola, C., and Smith, G.A., 2012, Fluvial morphology and sediment-flux of axial-transverse boundaries in an experimental basin: Journal of Sedimentary Research, v. 82, p. 310-325.

Dade, W.B., and Friend, P.F., 1998, Grain-size, sediment transport regime, and channel slope in alluvial rivers: Journal of Geology, v. 106, p. 661–675.

DeCelles, P.G., Gray, M.B., Ridgway, K.D., Cole, R.B., Srivastava, P.N., and Pivnik, D.A., 1991, Kinematic history of a foreland uplift from Paleocene synorogenic conglomerate, Beartooth Range , Wyoming and Montana: Geological Society of America, Bulletin, v. 103, p. 1458–1475.

DeCelles, P.G., 2004, Late Jurassic to Eocene evolution of the Cordilleran thrust belt and foreland basin system, western U.S.A.: American Journal of Science, v. 304, p. 105–168.

Dickinson, W.R., Klute, M.A., Hayes, M.J., Janecke, S.U., Erik, R., Mckittrick, M.A., Olivares, M.D., Klute, M.A., and Hayes, M.J., 1988, Paleogeographic and paleotectonic setting of Laramide sedimentary basins in the central Rocky Mountain region: Geological Society of America, Bulletin, v. 100, p. 1023–1039.

Dzombak, R., Midttun, N.C., Stein., R.A. and Sheldon, N.D., 2021, Incorporating lateral variability and extent of paleosols into proxy uncertainty: Palaeogeography, Palaeoclimatology, Paleoecology, v. 585, p. 1-12.

630 Duller, R.A., Armitage, J.J., Manners, H.R., Grimes, S., and Jones, T.D., 2019, Delayed sedimentary
631 response to abrupt climate change at the Paleocene-Eocene boundary, northern Spain:
632 Geology, v. 47, p. 159–162.

633 Fan, M., and Carrapa, B., 2014, Late Cretaceous – early Eocene Laramide uplift, exhumation, and
634 basin subsidence in Wyoming: Crustal responses to flat slab subduction: Tectonics, v. 33, p.
635 509–529.

636 Fielding, C.R., Allen, J.P., Alexander, J., and Gibling, M.G., 2009, Facies model for fluvial systems in the
637 seasonal tropics and subtropics: Geology, v. 37, p. 623–626.

638 Foreman, B.Z., 2014, Climate-driven generation of a fluvial sheet sand body at the Paleocene-Eocene
639 boundary in north-west Wyoming (USA): Basin Research, v. 26, p. 225–241.

640 Fricke, H.C., Clyde, W.C., O'Neil, J.R., and Gingerich, P.D., 1998, Evidence for rapid climate change in
641 North America during the latest Paleocene thermal maximum: oxygen isotope compositions
642 of biogenic phosphate from the Bighorn Basin (Wyoming): Earth and Planetary Science
643 Letters, v. 160, p. 193–208.

644 Ganti, V. Hajek, E.A., Leary, K., Straub., K.M., and Paola, C., 2020, Morphodynamic hierarchy and the
645 fabric of the sedimentary record: Geophysical Research Letters, v. 47, p. 1-10.

646 Gibling, M.R., 2006, Width and thickness of fluvial channel Bodies and valley fills in the geological
647 record: A literature compilation and classification: Journal of Sedimentary Research, 76, p.
648 731–770.

649 Gingerich, P.D., 2001, Biostratigraphy of the continental Paleocene-Eocene boundary internval on
650 Polecat Bench in the northern Bighorn Basin, *In* Gingerich, P.D (ed) Paleocene-Eocene

Stratigraphy and Biotic change in the Bighorn Basin and Clarks Fork Basins, Wyoming: University of Michigan, Papers on Paleontology, v. 33, p. 37-71.

Gingerich, P.D., 2003, Mammalian responses to climate change at the Paleocene-Eocene boundary: Polecat Bench record in the northern Bighorn Basin, Wyoming, *in* Wing, S.L., Gingerich, P.D., Schmitz, B., and Thomas, E., (eds.): Causes and Consequences of Globally Warm Climates in the Early Paleogene: Boulder, Colorado, Geological Society of America Special Paper 369, p. 463–478. Gingerich, P.D., and Clyde, W.C., 2001, Overview of mammalian biostratigraphy in the Paleocene-Eocene Fort Union and Willwood Formations of the Bighorn and Clarks Fork Basins: University of Michigan Papers on Paleontology, v. 33, p. 1–14.

IPCC, 2021: Climate Change 2021: The Physical Science Basis. Contribution of Working Group I to the Sixth Assessment Report of the Intergovernmental Panel on Climate Change [Masson-Delmotte, V., P. Zhai, A. Pirani, S.L. Connors, C. Péan, S. Berger, N. Caud, Y. Chen, L. Goldfarb, M.I. Gomis, M. Huang, K. Leitzell, E. Lonnoy, J.B.R. Matthews, T.K. Maycock, T. Waterfield, O. Yelekçi, R. Yu, and B. Zhou (eds.)]. Cambridge University Press, Cambridge, United Kingdom and New York, NY, USA, 2391 .p.

IPCC, 2022: Climate Change 2022: Impacts, Adaptation and Vulnerability. Contribution of Working Group II to the Sixth Assessment Report of the Intergovernmental Panel on Climate Change [H.-O. Pörtner, D.C. Roberts, M. Tignor, E.S. Poloczanska, K. Mintenbeck, A. Alegría, M. Craig, S. Langsdorf, S. Löschke, V. Möller, A. Okem, B. Rama (eds.)]. Cambridge University Press. Cambridge University Press, Cambridge, UK and New York, NY, USA, 3056 .p.

Jerolmack, D.J., and Paola, C., 2010, Shredding of environmental signals by sediment transport: Geophysical Research Letters, v. 37, p. 1–5.

673 Jones, H.L.L., and Hajek, E.A., 2007, Characterizing avulsion stratigraphy in ancient alluvial deposits:
674 Sedimentary Geology, v. 202, p. 124–137.

675 Knighton, D., 1998, Fluvial Forms and Processes: New Perspectives: Routledge, 400 p.

676 Kraus, M.J., 2001, Sedimentology and depositional setting of the Willwood Formation in the Bighorn
677 and Clarks Fork Basins, *in* Gingerich, P.D. (ed): Paloecene-Eocene Stratigraphy and biotic
678 Change in the Bighorn and Clarks Fork Basins, Wyoming, University of Michigan, Papers on
679 Paleontology, V. 33, p. 15-28.

680 Kraus, M.J., McInerney, F.A., Wing, S.L., Secord, R., Baczynski, A.A., and Bloch, J.I., 2013,
681 Paleohydrologic response to continental warming during the Paleocene–Eocene Thermal
682 Maximum, Bighorn Basin, Wyoming: Palaeogeography, Palaeoclimatology, Palaeoecology, v.
683 370, p. 196–208.

684 Kraus, M.J., and Wells, T.M., 1999, Recognizing avulsion deposits in the ancient stratigraphical record,
685 *in* Smith, N.D. and Rogers, J. (eds)., Fluvial Sedimentology 6: Special Publication of the
686 International Association of Sedimentologists, p. 251–268.

687 Kraus, M.J., and Riggins, S., 2007, Transient drying during the Paleocene–Eocene Thermal Maximum
688 (PETM): Analysis of paleosols in the bighorn basin, Wyoming: Palaeogeography,
689 Palaeoclimatology, Palaeoecology, v. 245, p. 444–461.

690 Kraus, M.J., Woody, D.T., Smith, J.J., and Dukic, V., 2015, Alluvial response to the Paleocene–Eocene
691 Thermal Maximum climatic event, Polecat Bench, Wyoming (U.S.A.): Palaeogeography,
692 Palaeoclimatology, Palaeoecology, v. 435, p. 177–192, doi:10.1016/j.palaeo.2015.06.021.

693 Leopold, L.B., and Maddock, T., 1953, The Hydraulic Geometry of Stream Channels and Some
694 Physiographic Implications: US Geological Survey, Professional Paper 252, 64 p.

695 Mackin, J.H., 1948, Concept of the graded river: Geological Society of America Bulletin, V. 59, p. 463-
696 512.

697 Macklin, M.G., Fuller, I.C., Lewin, J., Maas, G.S., Passmore, D.G., Rose, J., Woodward, J.C., Black, S.,
698 Hamlin, R.H.B., and Rowan, J.S., 2002, Correlation of fluvial sequences in the Mediterranean
699 basin over the last 200 ka and their relationship to climate change: Quaternary Science
700 Reviews, v. 21, p. 1633–1641.

701 Macklin, M.G., Lewin, J., and Woodward, J.C., 2012, The fluvial record of climate change: Royal
702 Society of London Philosophical Transactions A: Mathematical, Physical and Engineering
703 Sciences, v. 370, p. 2143–2172.

704 McInerney, F.A., and Wing, S.L., 2011, The Paleocene-Eocene Thermal Maximum: A Perturbation of
705 Carbon Cycle, Climate, and Biosphere with Implications for the Future: Annual Review of
706 Earth and Planetary Sciences, v. 39, p. 489–516.

707 Nanson, G.C., Cohen, T.J., Doyle, C.J. and Price, D.M., 2003, Alluvial evidence of major late Quaternary
708 climate and flow-regime changes on the coastal rivers of New South Wales, Australia, *in*: Gregory,
709 K. and Benito, G (eds.): Palaeohydrology: Understanding Global Change: John Wiley and
710 Sons, Chichester, p. 233– 258.

711 Middleton, G.V., 1973, Johannes Walther's Law of the Correlation of Facies: Geological Society of
712 America, Bulletin, V. 84, p. 979-988.

713 Owen, A., Ebinghaus, A., Hartley, A.J., Santos, M.G.M., and Weissmann, G.S., 2017, Multi-scale
714 classification of fluvial architecture: An example from the Palaeocene-Eocene Bighorn Basin,
715 Wyoming: Sedimentology, v. 64, p. 1572-1596.

716 Owen, A., Hartley, A.J., Ebinghaus, A., Weissmann, G.S., and Santos, M.G.M., 2019, Basin-scale
717 predictive models of alluvial architecture: Constraints from the Palaeocene–Eocene, Bighorn
718 Basin, Wyoming, USA: Sedimentology, v. 66, p. 736–763.

719 Pancost, R.D., 2017, Climate change Narratives: Nature Geoscience, v. 10, p. 466-468.

720 Paola, C., Ganti, V., Mohrig, D., Runkel., A.C., and Straub, K.M., 2018, Time not our time: Physical
721 controls on the preservation and measurement of geologic time: Annual Review of Earth and
722 Planetary Sciences, V. 46, p. 409-438.

723 Plink-Björklund, P., 2015, Morphodynamics of rivers strongly affected by monsoon precipitation:
724 Review of depositional style and forcing factors: Sedimentary Geology, v. 323, p. 110-147.

725 Rose, K.D., Chew, A.E., Dunn, R.H., Kraus, M.J., Fricke, H.C., and Zack, S.P. 2012, Earliest Eocene
726 Mammalian Fauna from the Paleocene-Eocene Thermal Maximum at Sand Creek Divide,
727 Southern Bighorn Basin, Wyoming: University of Michigan, Papers on Paleontology v. 36). P.
728 1-14.

729 Rouse, J.T., 1937, Genesis and structural relationships of the Absaroka volcanic rocks, Wyoming:
730 Geological Society of America Bulletin , v. 48, p. 1257–1296.

731 Ruhe, R.V. and Olson, C.G. 1980 Soil Welding: Soil Science, v. 130, p. 132-139.

732 Sadler, P.M., 1981, Sediment Accumulation Rates and the Completeness of Stratigraphic Sections:
733 Journal of Geology, v. 89, p. 569–584.

734 Schmitz, B., and Pujalte., V., 2003, Sea-level, humidity, and land-erosion records across the initial
735 Eocene thermal maximum from a continental-marine transect in northern Spain: Geology, v
736 31, p.689-692.

737 Schumm, S.A., 1979, Geomorphic Thresholds: The Concept and Its Applications: Institute of British
738 Geographers Transactions, v. 4, p. 485-515.

739 Seeland, D., 1998, Late Cretaceous , Paleocene, and Early Eocene Paleogeography of the Bighorn
740 Basin and Northwestern Wyoming, i*n*: Cretaceous and Lower tertiary Rocks of the Bighorn
741 Basin, Wyoming and Montana; 49th Annual Field Conference Guidebook, 1–29.

742 Simpson, G., and Castelltort, S., 2012, Model shows that rivers transmit high-frequency climate cycles
743 to the sedimentary record: Geology, v. 40, p. 1131–1134.

744 Slater, L.J., and Singer, M.B., 2013, Imprint of climate and climate change in alluvial riverbeds:
745 Continental United States, 1950-2011: Geology, v. 41, p. 595–598.

746 Smith, J.J., Hasiotis, S.T., Kraus, M.J., and Woody, D.T., 2008, Relationship of Floodplain
747 Ichnocoenoses to Paleopedology, Paleohydrology, and Paleoclimate in the Willwood
748 Formation, Wyoming, During the Paleocene-eocene Thermal Maximum: Palaios, v. 23, p.
749 683–699.

750 Snell, K.E., Thrasher, B.L., Eiler, J.M., Koch, P.L., Sloan, L.C., and Tabor, N.J., 2013, Hot summers in the
751 Bighorn Basin during the early Paleogene: Geology, v. 41, p. 55–58.

752 Snyder, W.S., Dickinson, W.R. and Silberman, M.L., 1976, Tectonic implications of space-time patterns
753 of Cenozoic magmatism in the Western United States: Earth and Planetary Science Letters, v.
754 32, p. 91-106.

Starkel, L., 1991, Environmental changes at the Younger Dryas-Preboreal transition and during the early Holocene: Some distinctive aspects in central Europe: The Holocene, v. 1, p. 234–242.

Straub, K.M., Duller, R.A., Foreman, B.Z., and Hajek, E.A., 2020, Buffered, Incomplete, and Shredded: The Challenges of Reading an Imperfect Stratigraphic Record: Journal of Geophysical Research: Earth Surface, v. 125, p. 1–44.

Sundell, K.A., 1990, Sedimentation and tectonics of the Absaroka Basin of northwestern Wyoming, *in* Wyoming sedimentation and Tectonics, 41st Annual Field Conference Guidebook, p. 105–122.

Toby, S.C., Duller, R.A., Angelis, S.D., and Straub, K.M., 2022, Morphodynamics limits to environmental signal propagation across landscape and into strata: Nature Communications, v. 12., 10. p.

Vandenberghe, J., 2002, the relation between climate and river processes, landforms and deposits during the Quaternary: Quaternary International, V.91, p.17-23.

Van Houten, F.B., 1944, Stratigraphy of the Willwood and Tatman Formations in northwestern Wyoming: Geological Society of America 1987 Annual Meeting and Exposition Program, v. 55, p. 165–210.

Welch, J.L., Foreman, B.Z., Malone, D., and Craddock, J., 2022, Provenance of early Paleogene strata in the Bighorn Basin (Wyoming, USA): Implications for Laramide tectonism and basin-scale stratigraphic patterns, *in* Craddock, J.P., Malone, D.H., Foreman, B.Z., and Konstantinou, A., (eds), Tectonic Evolution of the Sevier-Laramide Hinterland, Thrust Belt, and Foreland, and Postorogenic Slab Rollback (180–20 Ma): Geological Society of America, Special Paper 555, p. 241–264

776 Whipple, K.X., 2001, Fluvial landscape response time: how plausible is steady-state denudation:
777 American Journal of Science, v. 301, p. 313–325.

778 Willis, B.J., and Behrensmeyer, A.K., 1995, Fluvial systems in the Siwalik Miocene and Wyoming
779 Paleogene: Palaeogeography, Palaeoclimatology and Palaeoecology, v. 115, p. 13-35.

780 Wing, S.L., and Currano, E.D., 2013, Plant response to a global greenhouse event 56 million years ago:
781 American Journal of Botany, v. 100, p. 1234–54.

782 Wing, S.L., Harrington, G.J., Smith, F.A., Bloch, J.I., Boyer, D.M., and Freeman, K.H., 2005, Transient
783 floral change and rapid global warming at the Paleocene-Eocene boundary: Science, v. 310, p.
784 993–6.

785 Yuretich, R.F., Hickey, L.J., Gregson, B.P., and Hsia, Y.L., 1984, Lacustrine deposits in the Paleocene
786 Fort Union Formation, northern Bighorn Basin, Montana: Journal of Sedimentary Petrology, v.
787 54, p. 836–852.

788 Zachos, J.C., Wara, M.W., Bohaty, S., Delaney, M.L., Petrizzo, M.R., Brill, A., Bralower, T.J., and
789 Premoli-Silva, I., 2003, A transient rise in tropical sea surface temperature during the
790 Paleocene-Eocene Thermal Maximum: Science, v. 302, p. 1551-1554.

791 Zachos, J.C., Röhol, U., Schellenberg, S.A., Sluijs, A. Hodell, D.A., Kelly, D.C., Thomas, E., Nicolo, M.,
792 Raffi, I., Lourens, L.J., McCarren, H., Kroon, D.2005, Rapid acidification of the ocean during the
793 Paleocene-Eocene Thermal Maximum: Science, v. 308, p. 1611–1616.

Figure 1

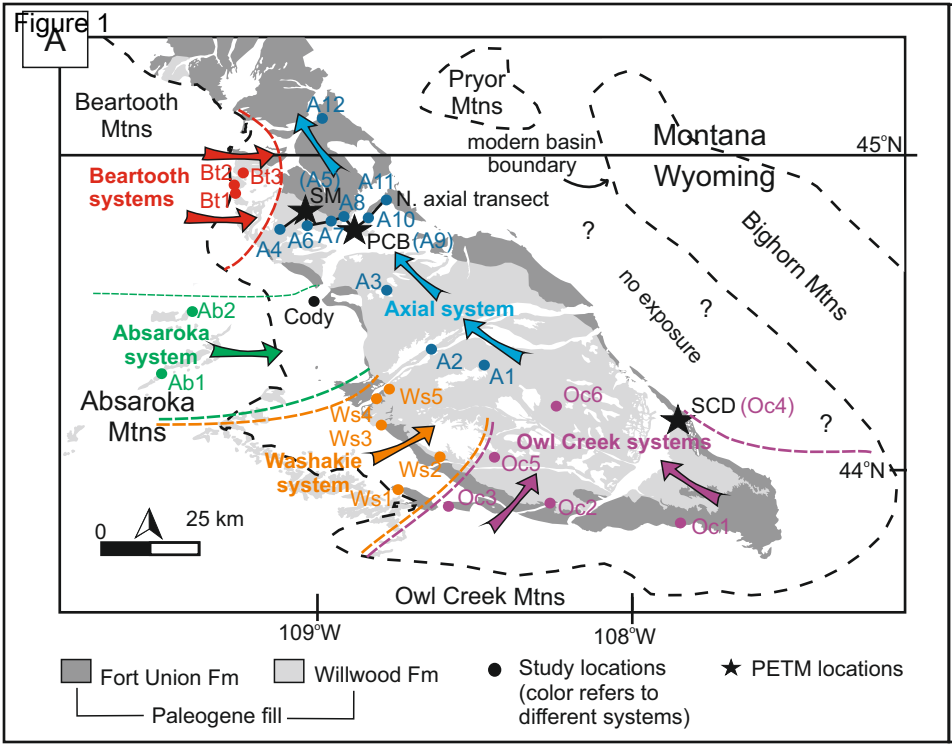

B

Epoch	Age (N.America)	Formation
Eocene	Bridgarton	No strat
		Tatman Fm
	Wasatchian	Willwood Fm
	Clarkforkian	
Paleocene	Tiffanian	Fort Union Fm
	Torrajonian	
	Puercan	

Figure 2

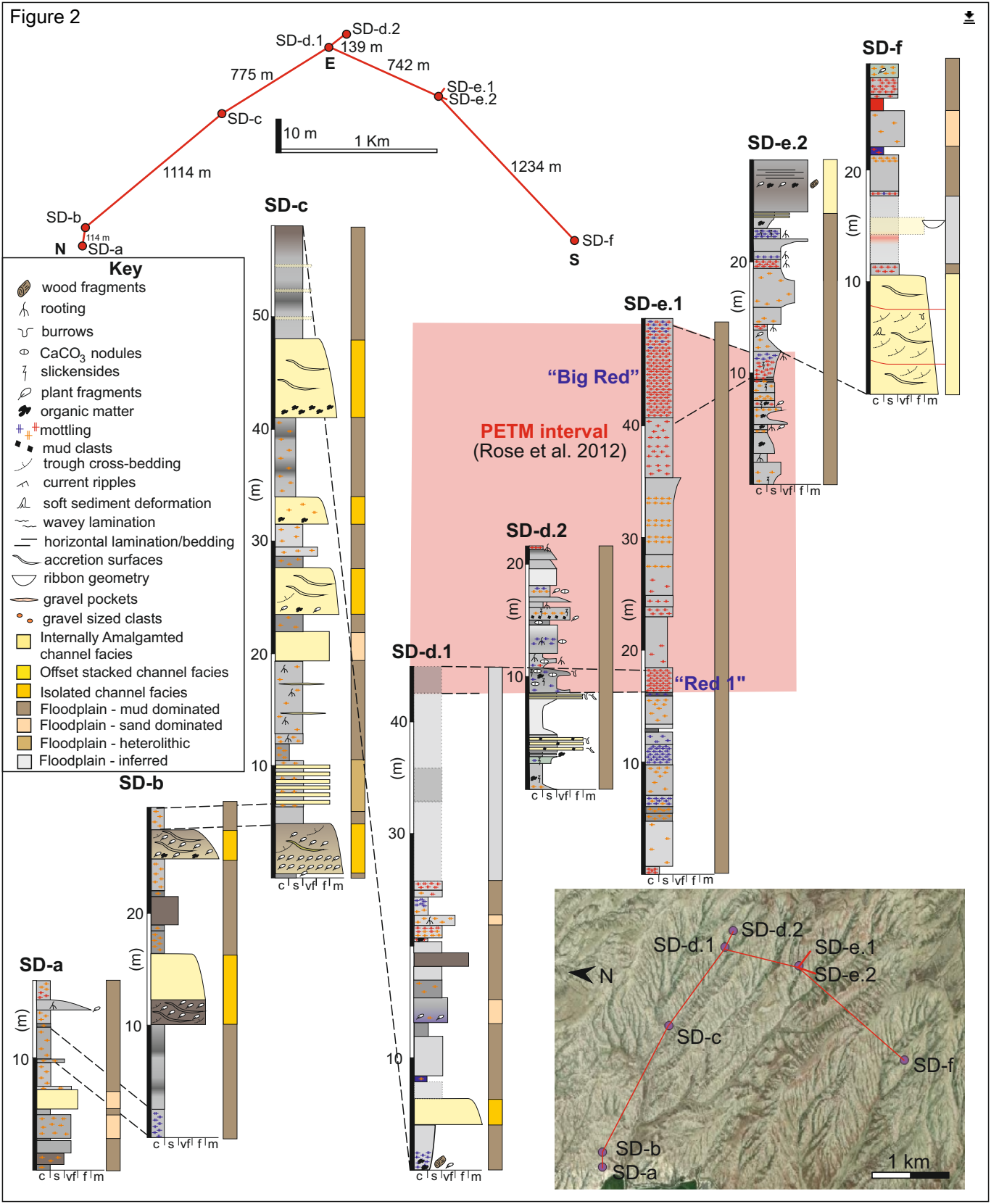
SD-d.1
SD-d.2
139 m
E
775 m
742 m
SD-e.1
SD-e.2
SD-c
10 m
1 Km
1114 m
1234 m
SD-b
114 m
N
SD-a
SD-f
S
Key
wood fragments
rooting
burrows
CaCO3 nodules
slickensides
plant fragments
organic matter
mottling
mud clasts
trough cross-bedding
current ripples
soft sediment deformation
wavey lamination
horizontal lamination/bedding
accretion surfaces
ribbon geometry
gravel pockets
gravel sized clasts
Internally Amalgamted channel facies
Offset stacked channel facies
Isolated channel facies
Floodplain - mud dominated
Floodplain - sand dominated
Floodplain - heterolithic
Floodplain - inferred
SD-c
SD-b
SD-a
SD-d.1
SD-d.2
SD-e.1
SD-e.2
SD-f
"Big Red"
PETM interval
(Rose et al. 2012)
"Red 1"
(m)
c s vf f m
N
1 km

Figure 3

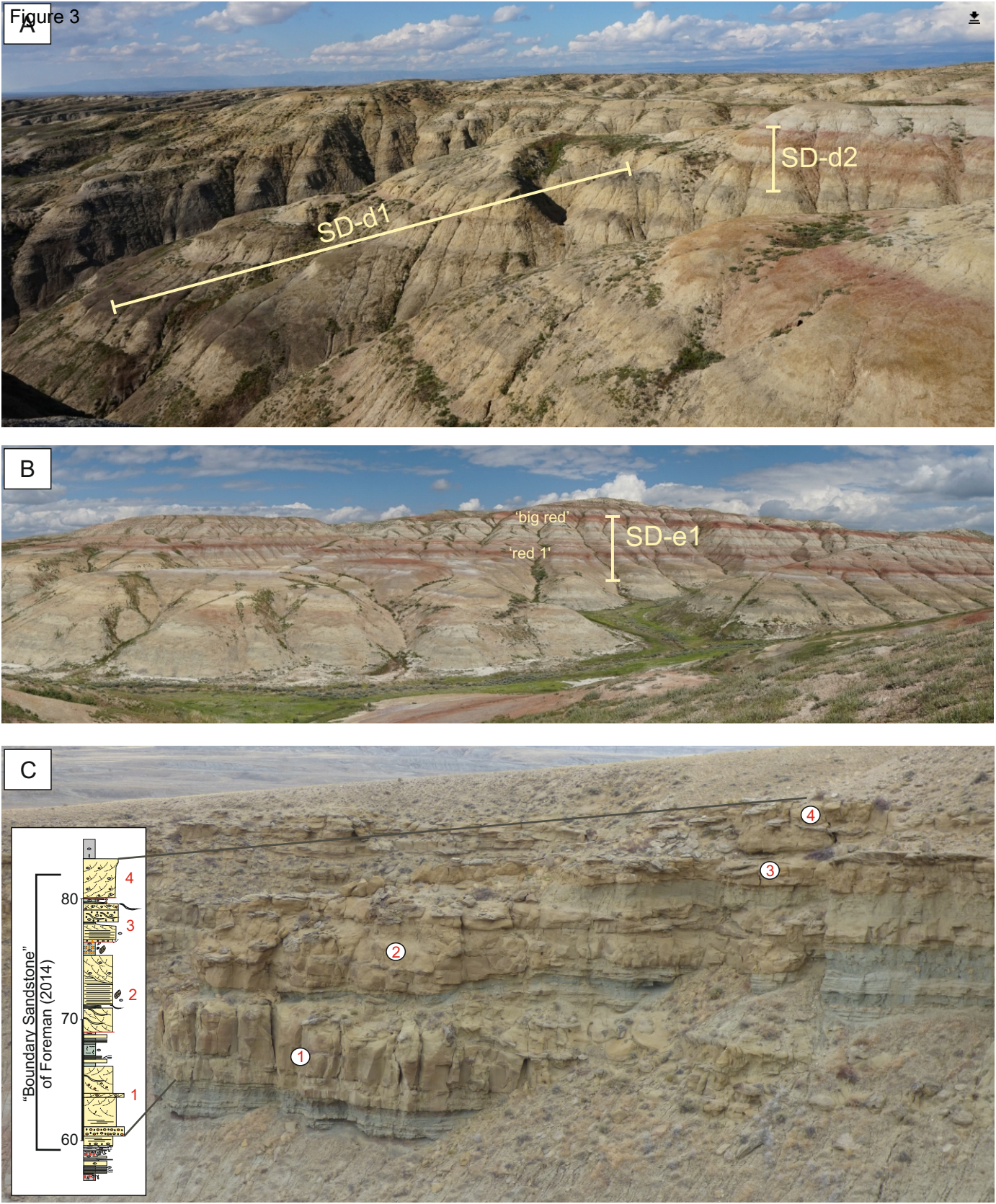
A
SD-d1
SD-d2
B
'big red'
'red 1'
SD-e1
C
"Boundary Sandstone" of Foreman (2014)
80
70
60
1
2
3
4

Figure 4

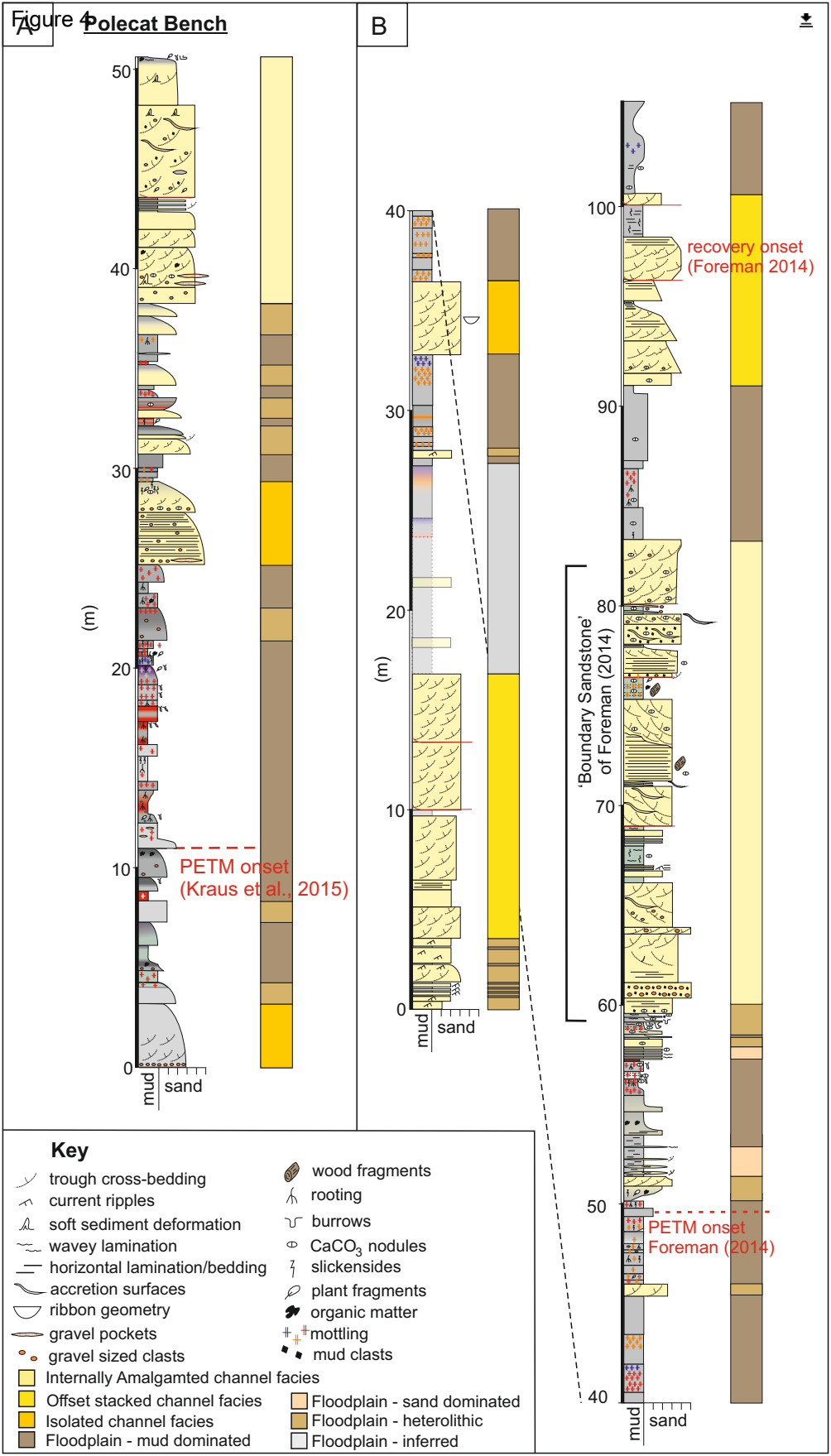
A
Polecat Bench
B
(m)
mud
sand
PETM onset
(Kraus et al., 2015)
recovery onset
(Foreman 2014)
'Boundary Sandstone'
of Foreman (2014)
PETM onset
Foreman (2014)
Key
trough cross-bedding
current ripples
soft sediment deformation
wavey lamination
horizontal lamination/bedding
accretion surfaces
ribbon geometry
gravel pockets
gravel sized clasts
wood fragments
rooting
burrows
CaCO3 nodules
slickensides
plant fragments
organic matter
mottling
mud clasts
Internally Amalgamted channel facies
Offset stacked channel facies
Isolated channel facies
Floodplain - mud dominated
Floodplain - sand dominated
Floodplain - heterolithic
Floodplain - inferred

Figure 5

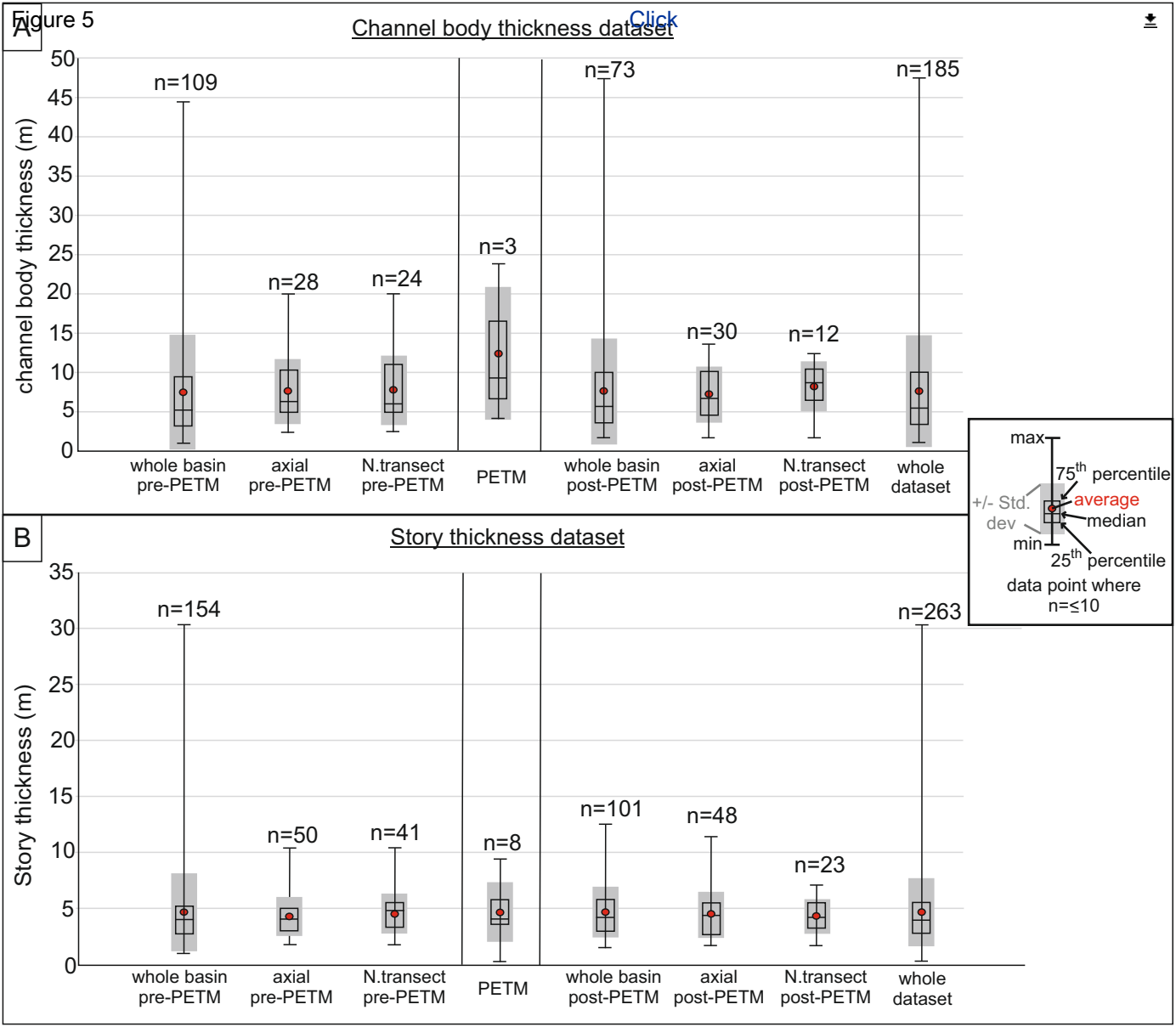
A
Click
Channel body thickness dataset
channel body thickness (m)
50
45
40
35
30
25
20
15
10
5
0
n=109
n=28
n=24
n=3
n=73
n=30
n=12
n=185
whole basin pre-PETM
axial pre-PETM
N.transect pre-PETM
PETM
whole basin post-PETM
axial post-PETM
N.transect post-PETM
whole dataset
max
75th percentile
+/- Std. dev
average
median
min
25th percentile
data point where n=≤10
B
Story thickness dataset
Story thickness (m)
35
30
25
20
15
10
5
0
n=154
n=50
n=41
n=8
n=101
n=48
n=23
n=263
whole basin pre-PETM
axial pre-PETM
N.transect pre-PETM
PETM
whole basin post-PETM
axial post-PETM
N.transect post-PETM
whole dataset

Figure 6

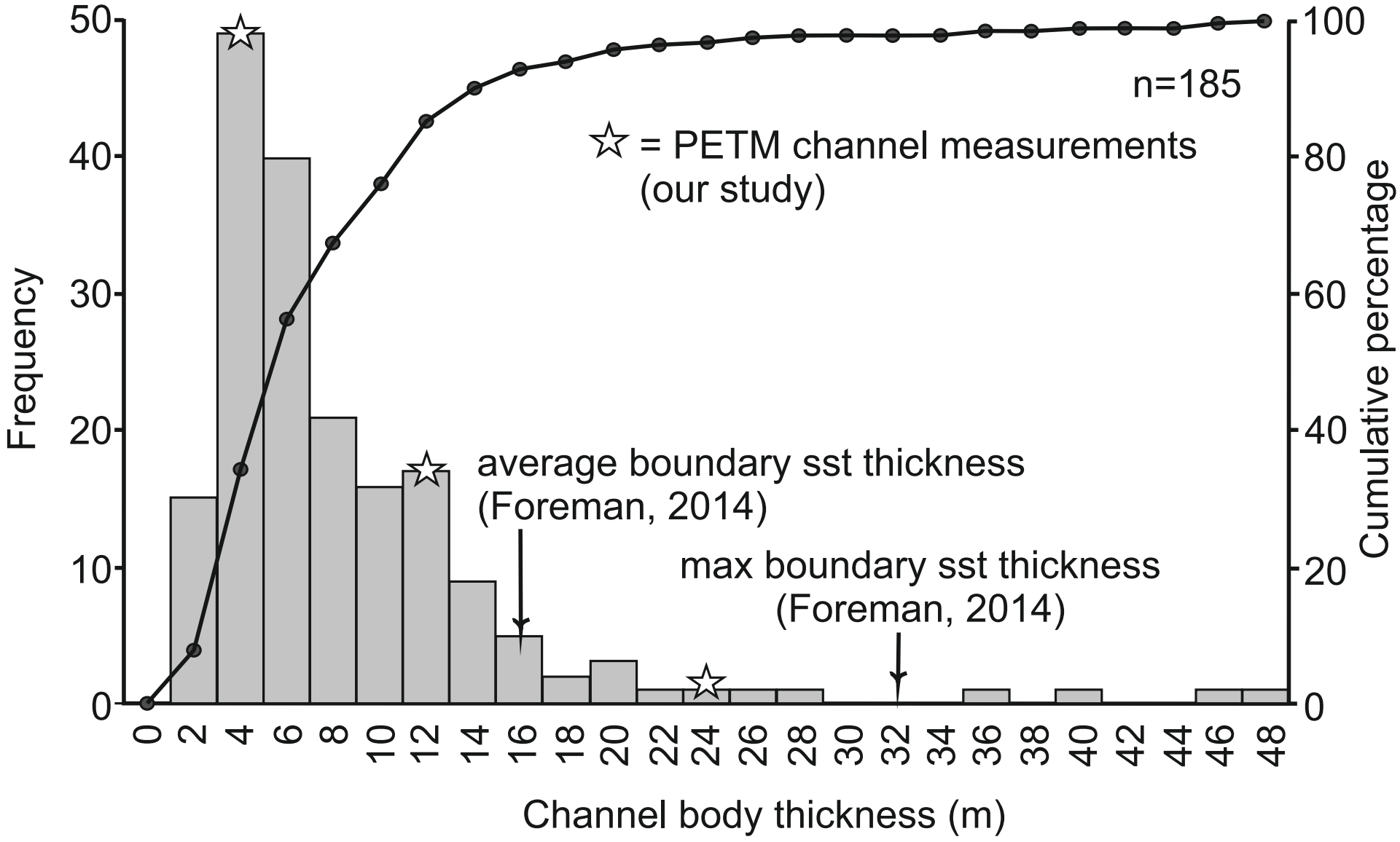
n=185
☆ = PETM channel measurements
(our study)
average boundary sst thickness
(Foreman, 2014)
max boundary sst thickness
(Foreman, 2014)
Frequency
Cumulative percentage
Channel body thickness (m)
0
10
20
30
40
50
0
20
40
60
80
100
0 2 4 6 8 10 12 14 16 18 20 22 24 26 28 30 32 34 36 38 40 42 44 46 48

Figure 7

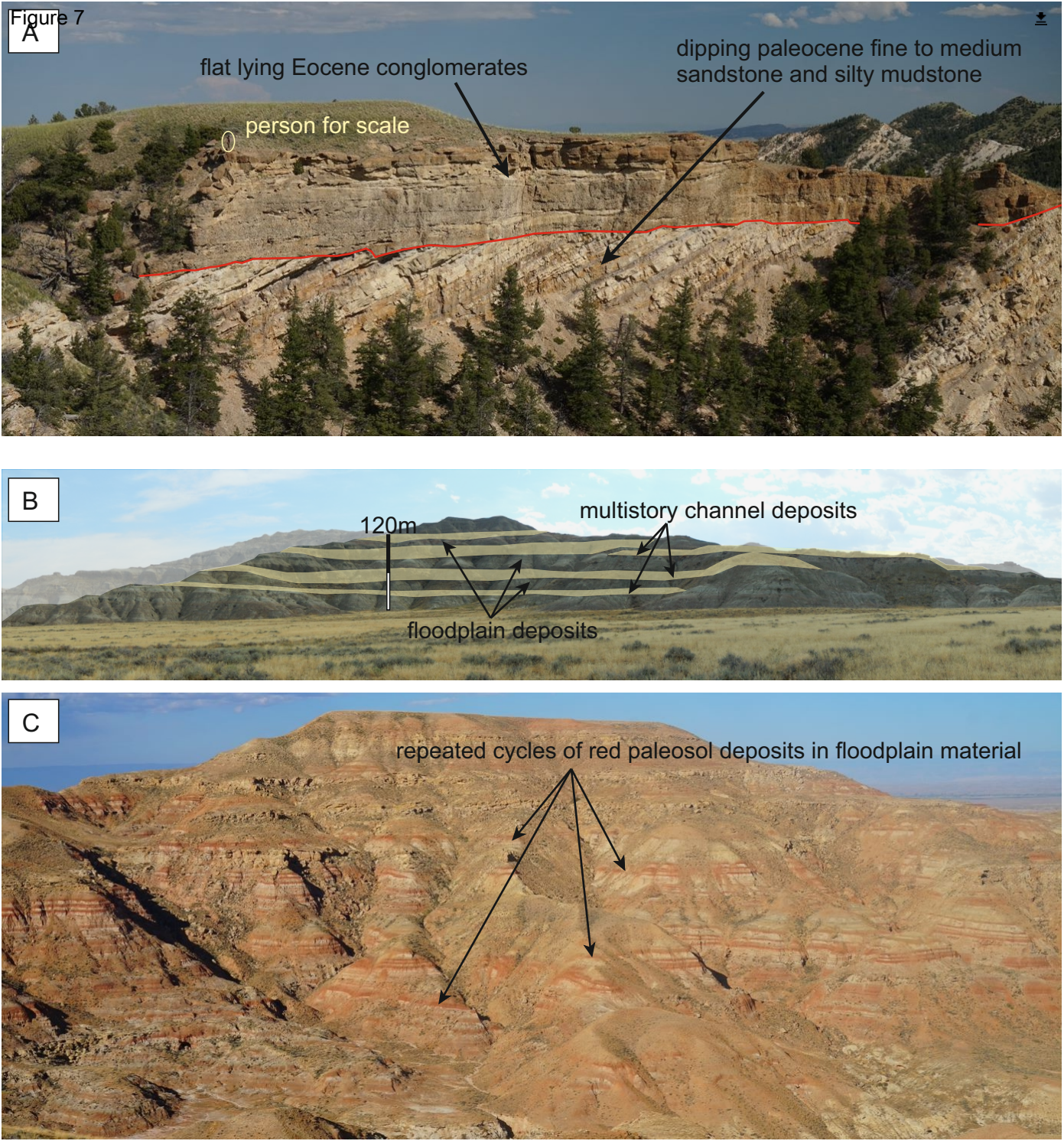
A
flat lying Eocene conglomerates
dipping paleocene fine to medium sandstone and silty mudstone
person for scale
B
120m
multistory channel deposits
floodplain deposits
C
repeated cycles of red paleosol deposits in floodplain material

Table 1. Summary of key characteristics and examples of pre-PETM, PETM, and post-PETM within the Bighorn Basin. Please see references for full details, examples and broad trends given in Table 1.

	Pre-PETM	PETM	Post-PETM
Mean annual temperature (MAT; °C) LMA, Wing et al., 2005)	15.7 ± 2.4 (Wing et al. 2005)	Increase of approximately 5 19.8 ± 3.1 (Wing et al. 2005)	18.2 ± 2.3 (Wing et al. 2005)
Mean annual precipitation (MAP; mm) LMA - Wing et al., 2005); CIA-K Paleosol analysis.Kraus and Riggins, 2007; Kraus et al., 2015)	1139-1163 ± 108 (Kraus and Riggins, 2007) 1153-1208 ± 108 (Kraus et al. 2015)	800+1140/–560 & 410 for base PETM. 1440 + 2060/−1000 & 1320 upper PETM (Wing et al., 2005) 755-1186 ± 108 (Kraus and Riggins, 2007) 516-1157 ± 108 (Kraus et al. 2015)	Pre-PETM values (e.g. 820-1036 ± 108; Kraus et al. 2015).
Vegetation type (Wing et al., 2005; Smith et al., 2008; McInerney and Wing, 2011; Kraus et al., 2013)	Deciduous and evergreen broad-leaved taxa, conifers in the bald cypress family. Mesic temperate environments	Lacks conifers, dominated by bean family. Dry tropical and subtropical setting.	Pre-PETM conditions
Vegetation density (Wing et al., 2005; Smith et al., 2008)	Dense forest structure	Relatively open/less dense forest structure	Pre-PETM conditions
Mammalian fauna (Gingerich, 2003)	*Champsosaurus*, Plesiadapidae. Appearance of Rodentia,Tillodontia, *Haplomylu in the Clarksforkian.*	"Dwarfing" of mammals. Appearance of new species e.g., the condylarth,the pantodont *Coryphodon.* Disappearance of *Champsosaurus*, Plesiadapidae.	Some species recover, some permanently change ("evolutionary change"). First appearance of cosmopolitan Perissodactyla,Artiodactyla, Primates, and hyaenodontid
Paleosols (Kraus and Riggins, 2007; Kraus et al., 2013; 2015)	Dominantly gray, intermittent thin purple/red paleolsols.	More welded and thicker red, yellow-brown	Intermediate paleosls. More widely spaced paleosols

Table 2 Summary descriptions of facies associations observed in the Paleocene and Eocene fill of the Bighorn Basin (see Owen et al., 2017 for full descriptions of facies and geometries.).

Channel body geometries (Owen et al., 2017)	**Massive**	Large, broad channel geometry. Rare story surfaces that are spatially isolated
	Semi Amalgamated	Semi-amalgamated with other channel deposits. Channel body can have irregular geometries. Story surfaces are present to varying degrees, can be crosscutting one another or spatially isolated.
	Internally amalgamated	Broad tabular geometry that laterally pinches out. Story surfaces are prevalent, can be crosscutting one another, or spatially isolated.
	Offset stacked	A broad tabular geometry. However, stories are offset from one another, leaving an irregular edge to the channel body. Single story across most of the channel body, multistory across minor portions at amalgamation points.
	Isolated	Channel geometry that pinches out laterally. Can be asymmetrical or symmetrical. Single story.
Channel facies association (Owen et al., 2017)	**Gravelly braided stream**	Conglomerates composed of granule- to boulder-sized, well-rounded, moderately sorted. Imbrication, fining-up sequences, sandstone lenses, accretion surfaces and parallel stratification can be present. Matrix composed of silt to coarse sand. Channel body can be either massive or semi-amalgamated.
	Heterolithic, dominantly braided	Medium- to cobble-dominated sandstone that are moderate to poorly sorted. Parallel lamination, trough cross bedding and accretion surfaces (dominantly downstream) present. Channel body can be Internally amalgamated, semi-amalgamated, or have massive geometries
	Heterolithic, dominantly meandering	Dominantly medium to fine sandstone. Well-sorted with area with material (mud, granules, or nodules) lining trough cross sets. Upper and lower plane-bed lamination, current ripples, accretion packages (dominantly lateral) and soft-sediment deformation present. Mudstone present in some heterolithic accretion packages. Channel bodies can have a semi-amalgamated, internally amalgamated, or offset-stacked geometry.
	Fine-grained channel fill	Silt to medium sandstone with deposits being either heterolithic, or sand- or mud-dominated. Current ripples, trough cross bedding and parallel lamination present. Rare accretion surfaces (dominantly lateral). Channel bodies can have an internally amalgamated, offset stacked or isolated geometry.
Floodplain deposits (Owen et al., 2017)	**Minor lacustrine**	Mud- to sand-dominated sequences with horizontal lamination, current ripples, bioturbation, and trough cross stratification present to varying degrees. Rare limestone beds with wavy lamination.
	Paleosols	Two broad paleosols types observed. Well-drained paleosols are dominantly red and composed of clay to fine to medium sandstone. Rootlets, rhizoliths, carbonate nodules, slickensides, mottling, organic matter and bioturbation all observed. Poorly drained deposits are gray, green, and purple and composed of clay to fine-medium sandstone. Structures include rootlets, slickensides, mottling, and burrows, but to a lesser degree than the well-drained paleosols, with the exception of organic matter, which is more prevalent in the poorly drained facies.
	Splay and sheet floods	Composed of minor channel (ribbon) and sheet deposits composed of fine to coarse sands that are well sorted. Structures present include parallel and ripple lamination and minor trough cross bedding as well as evidence of bioturbation.

Table 3 Summary data (in meters) for channel body and storey deposits pre-PETM, PETM and post-PETM for the whole basin, whole axial system and northern basin transect. See Figure 5 for graphical representation of dataset.

Channel bodies								
	whole Basin Pre-PETM	**whole axial pre-PETM)**	**north basin pre-PETM**	**PETM**	**whole basin post-PETM**	**axial post-PETM**	**north basin post-PETM**	**Entire dataset**
Average thickness (m)	7.49	7.65	7.75	12.40	7.66	7.19	8.25	7.64
Max thickness (m)	44.50	20.00	20.00	23.80	47.50	13.70	12.40	47.50
Min thickness (m)	1.00	2.40	2.40	4.10	1.70	1.70	1.70	1.00
Upper stdv (m)	14.71	11.71	12.08	20.74	14.27	10.64	11.34	14.67
Lower stdv (m)	0.27	3.59	3.42	4.06	1.04	3.74	5.16	0.60
Q1 (m)	3.20	4.95	4.95	6.70	3.60	4.53	6.48	3.40
Median (m)	5.20	6.30	6.00	9.30	5.70	6.75	8.70	5.50
Q3 (m)	9.40	10.25	11.00	16.55	10.10	10.15	10.40	10.00
Stories								
	whole Basin Pre-PETM	**whole axial pre-PETM)**	**north basin pre-PETM**	**PETM**	**whole basin post-PETM**	**axial post-PETM**	**north basin post-PETM**	**Entire dataset**
Average thickness (m)	4.67	4.29	4.54	4.65	4.67	4.50	4.30	4.67
Max thickness (m)	30.30	10.40	10.40	9.40	12.50	11.40	7.10	30.30
Min thickness (m)	1.00	1.80	1.80	0.30	1.50	1.70	1.70	0.30
Upper stdv (m)	8.08	5.96	6.26	7.24	6.87	6.46	5.77	7.64
Lower stdv (m)	1.26	2.61	2.81	2.06	2.47	2.53	2.84	1.69
Q1 (m)	2.73	3.00	3.30	3.60	3.00	2.75	3.25	3.00
Median (m)	4.00	4.05	4.80	4.05	4.20	4.40	4.20	4.00
Q3 (m)	5.20	5.00	5.50	5.75	5.80	5.50	5.50	5.50

Table 4. Summary statistical results comparing pre-PETM and PETM channel depths (storey thicknesses). Results are presented for two assumptions for standard deviations, s.d., for the PETM data: (1) s.d. calculated from all 8 available measurements; (2) s.d. estimated as being the same as in the larger pre-PETM data sets for the same locations. The channel-forming discharge estimates were calculated using f=0.4 in an empirical relationship between channel depth, h, and discharge, Q, $h=cQ^f$.

	Northern Axial		Axial	
	Pre-PETM	PETM	Pre-PETM	PETM
Number of measurements, N	41	8	50	8
Mean $\overline{x}$ $[m]$	4.54	4.65	4.29	4.65
Standard deviation σ [m]	1.73	2.77	1.68	2.77
Standard error, s.e., ($\overline{x}/\sqrt{N}$) [m]	0.27	0.98	0.24	0.98
Pooled s.e. (measured / estimated PETM σ)	1.01 / 0.67		1.01 / 0.64	
t-values (calculated / critical at 95% confidence)	0.11 / 1.90		0.36 / 1.90	
Minimum PETM storey thickness for 95% significant increase (using measured / estimated PETM σ)	6.46 / 5.80		6.19 / 5.49	
Ratio of channel-forming discharge Q during PETM to pre-PETM to produce 95% significant channel depth increase (using measured / estimated PETM σ)	2.42 / 1.85		2.51 / 1.86	

Beartooth fluvial systems

KEY

- current ripples
- horizontal lamination
- trough cross-bedding
- wavey lamination
- slumping
- imbricated clasts
- accretion surface
- gravel lense
- sand lense
- soft sediment deformation
- mud clast
- outsized clast
- granule
- channel geomoetry
- gradational boundary
- storey surface
- wood debris
- rootlets
- vertical burrow
- sub-horizontal burrow
- horizontal burrow
- groove
- bone material
- shell material
- slickensides
- calcium carbonate nodule
- leaf material
- mottling
- organic material
- Massive channel facies
- Semi-Amalgamated channel facies
- Internally Amalgamted channel facies
- Offset stacked channel facies
- Isolated channel facies
- Floodplain - mud dominated
- Floodplain - sand dominated
- Floodplain - heterolithic
- Floodplain channel (splay)
- Floodplain- inferred

Please see Owen et al. 2017 for full facies descriptions

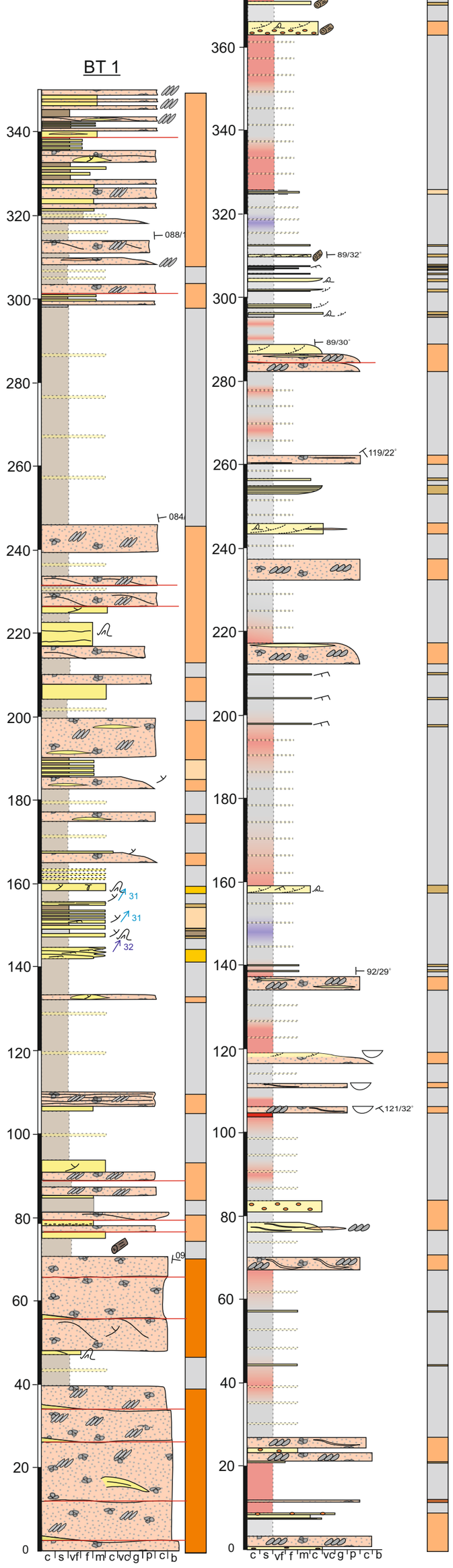

Absoraka fluvial systems

KEY

- current ripples
- horizontal lamination
- trough cross-bedding
- wavey lamination
- slumping
- imbricated clasts
- accretion surface
- gravel lense
- sand lense
- soft sediment deformation
- mud clast
- outsized clast
- granule
- channel geomoetry
- gradational boundary
- storey surface
- wood debris
- rootlets
- vertical burrow
- sub-horizontal burrow
- horizontal burrow
- groove
- bone material
- shell material
- slickensides
- calcium carbonate nodule
- leaf material
- mottling
- organic material
- Massive channel facies
- Semi-Amalgamated channel facies
- Internally Amalgamted channel facies
- Offset stacked channel facies
- Isolated channel facies
- Floodplain - mud dominated
- Floodplain - sand dominated
- Floodplain - heterolithic
- Floodplain channel (splay)
- Floodplain- inferred

Please see Owen et al. 2017 for full facies descriptions

AB 1

AB 2

faulted section

c s vf f m c vc g p

Washakie fluvial systems

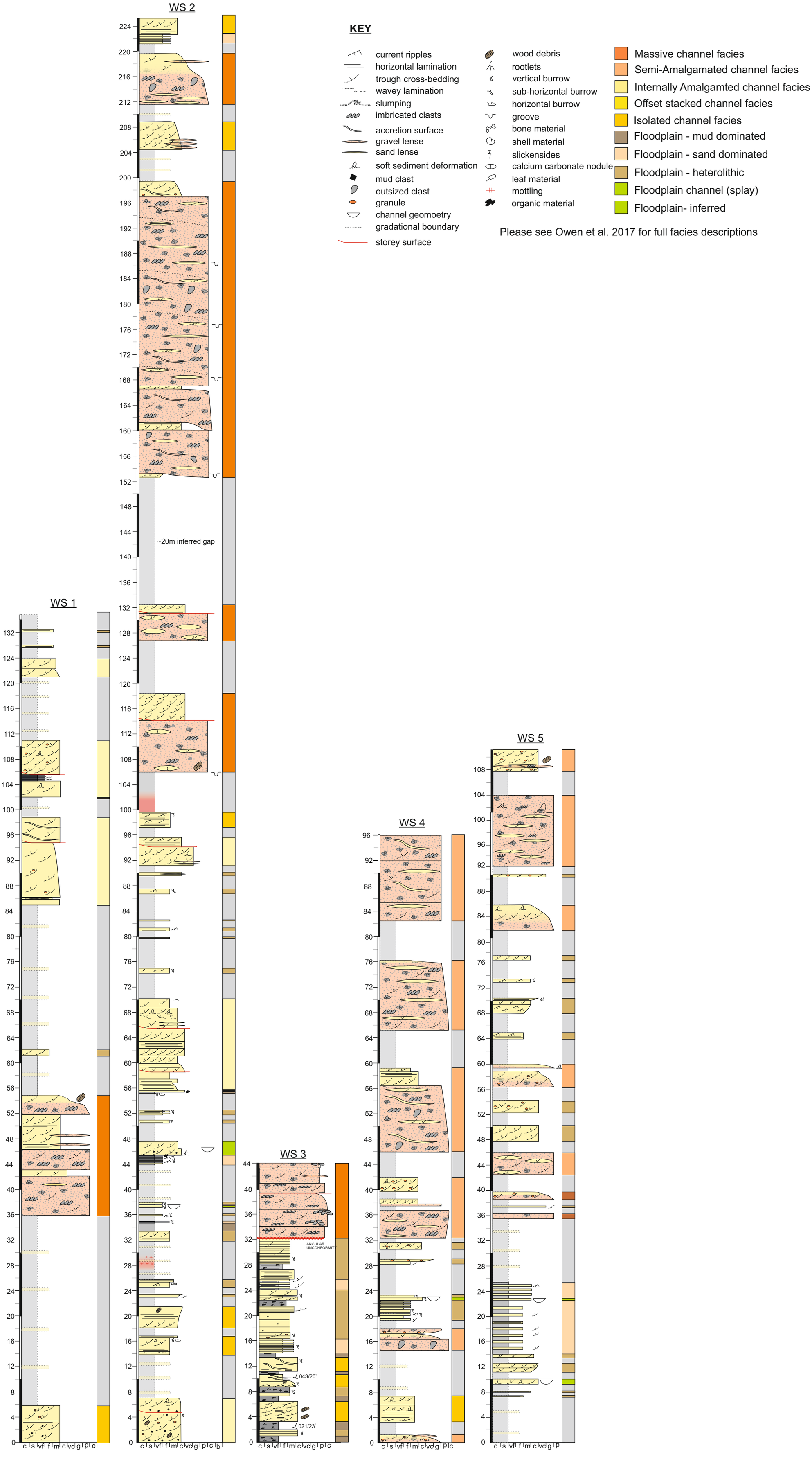

Owl Creek System

KEY

- current ripples
- horizontal lamination
- trough cross-bedding
- wavey lamination
- slumping
- imbricated clasts
- accretion surface
- gravel lense
- sand lense
- soft sediment deformation
- mud clast
- outsized clast
- granule
- channel geomoetry
- gradational boundary
- storey surface
- wood debris
- rootlets
- vertical burrow
- sub-horizontal burrow
- horizontal burrow
- groove
- bone material
- shell material
- slickensides
- calcium carbonate nodule
- leaf material
- mottling
- organic material
- Massive channel facies
- Semi-Amalgamated channel facies
- Internally Amalgamted channel facies
- Offset stacked channel facies
- Isolated channel facies
- Floodplain - mud dominated
- Floodplain - sand dominated
- Floodplain - heterolithic
- Floodplain channel (splay)
- Floodplain- inferred

Please see Owen et al. 2017 for full facies descriptions

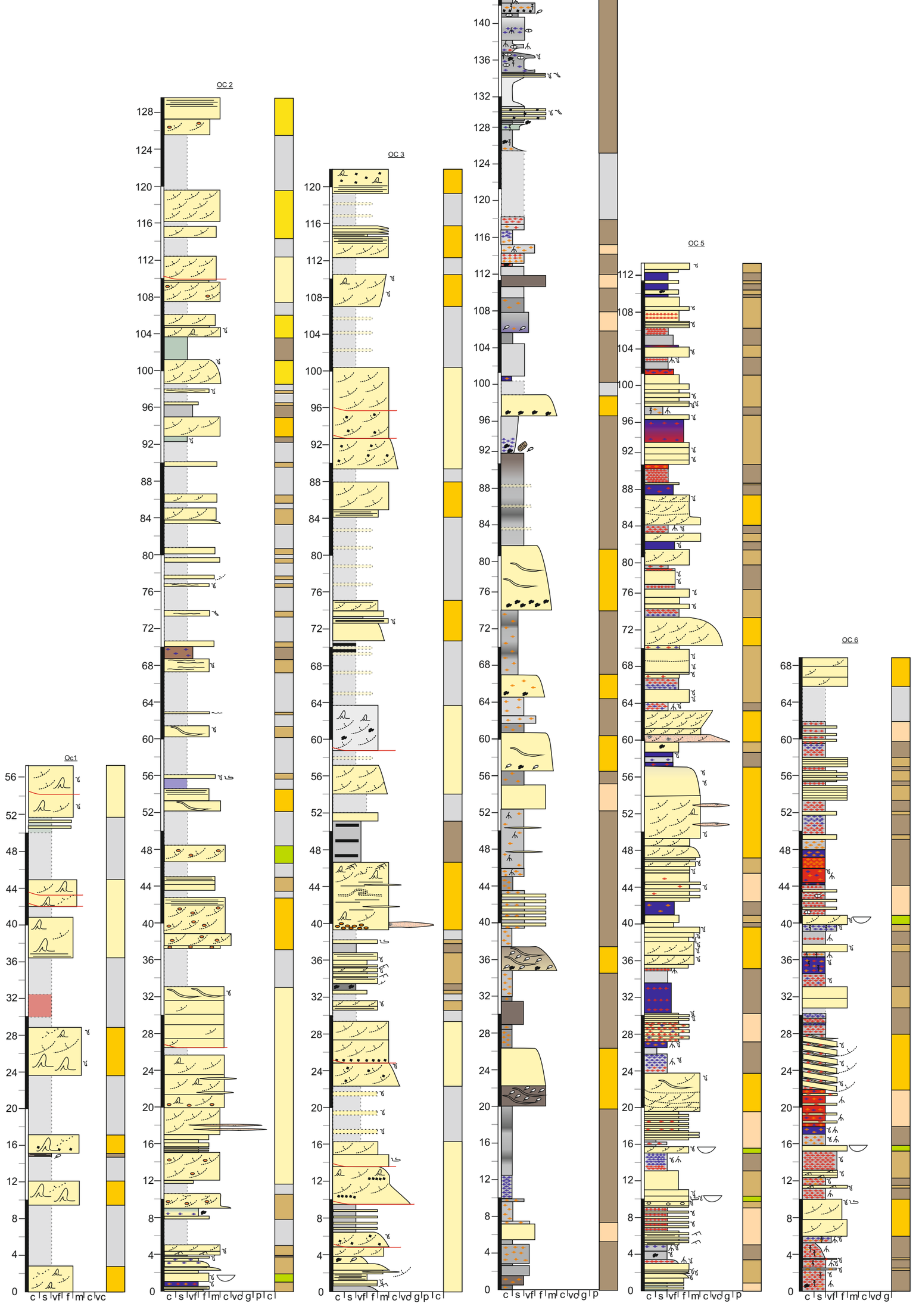

Axial fluvial system

KEY

- current ripples
- horizontal lamination
- trough cross-bedding
- wavey lamination
- slumping
- imbricated clasts
- accretion surface
- gravel lense
- sand lense
- soft sediment deformation
- mud clast
- outsized clast
- granule
- channel geomoetry
- gradational boundary
- storey surface
- wood debris
- rootlets
- vertical burrow
- sub-horizontal burrow
- horizontal burrow
- groove
- bone material
- shell material
- slickensides
- calcium carbonate nodule
- leaf material
- mottling
- organic material
- Massive channel facies
- Semi-Amalgamated channel facies
- Internally Amalgamted channel facies
- Offset stacked channel facies
- Isolated channel facies
- Floodplain - mud dominated
- Floodplain - sand dominated
- Floodplain - heterolithic
- Floodplain channel (splay)
- Floodplain- inferred

Please see Owen et al. 2017 for full facies descriptions

A 1 A 2 A 3 A 4 A 5 A 6 A 7 A 8 A 9 A 10 A 11 A 12